SEQUENTIAL STATE-PARAMETER ESTIMATION FOR PARABOLIC PROBLEMS USING PARTICLE FILTER WITH THE METHOD OF FUNDAMENTAL SOLUTIONS

CARLOS EDUARDO POLATSCHEK KOPPERSCHMIDT

Vitória - ES

February 2020

CARLOS EDUARDO POLATSCHEK KOPPERSCHMIDT

SEQUENTIAL STATE-PARAMETER ESTIMATION FOR PARABOLIC PROBLEMS USING PARTICLE FILTER WITH THE METHOD OF FUNDAMENTAL SOLUTIONS

Master's degree dissertation presented to *Programa de Pós-Graduação em Engenharia Mecânica* from UFES as requirement to obtain the title of Master in Mechanical Engineering.

Universidade Federal do Espírito Santo – UFES
Centro Tecnológico
Programa de Pós-Graduação em Engenharia Mecânica – PPGEM

First Adviser: Prof. Dr. Wellington Betencurte da Silva
Second Adviser: Prof. Dr. Júlio César Sampaio Dutra

Vitória - ES
February 2020

CARLOS EDUARDO POLATSCHEK KOPPERSCHMIDT

SEQUENTIAL STATE-PARAMETER ESTIMATION FOR PARABOLIC PROBLEMS USING PARTICLE FILTER WITH THE METHOD OF FUNDAMENTAL SOLUTIONS

Master's degree dissertation presented to Programa de Pós-Graduação em Engenharia Mecânica from UFES as requirement to obtain the title of Master in Mechanical Engineering.

Dr. Wellington Betencurte da Silva - UFES
First Adviser

Dr. Júlio César Sampaio Dutra - UFES
Second Adviser

Dr. Márcio Ferreira Martins - PPGEM/UFES

Dr. José Mir Justino da Costa - UFAM

ACKNOWLEDGEMENTS

This work is dedicated to my family, specially to my mother and my father. I thank Wellington Betencurte, and Júlio Dutra, my advisors, for their support and encouragement. Thanks to Bruno Margotto, my friend and Master’s degree partner. I appreciate the FAPES for the financial support and thank to PPGEM for the opportunity to take a big step in my personal and professional life.

"All is flux."

(Heraclitus)

ABSTRACT

Thermal processes related to most of practical problems involve the need to be investigated as inverse problems. In this aspect, the implementation of numerical or analytical-numerical solutions is essential because of complexity in obtaining purely analytical solutions, and this requires fast and accurate responses. This present work addresses, in the context of parabolic heat conduction problems, the Method of Fundamental Solutions (MFS) numerical approximations combined with Bayesian procedures for state and parameter estimating. In the MFS we consider the fundamental solution of the parabolic heat equation in order to solve the time-dependent term together with the resulting system of equations, without needing to perform que transformation of the Parabolic equation into Elliptic, therefore it does not require treating the time component separately. The cases presented consist of homogeneous problems whose solution is previously known, in order to assess the proposed method behavior for different situations. The investigated problems were based on Robin boundary to one and two-spatial dimensions and one dimension for the time. The method is easily extensible to higher dimension problems. Problems were also investigated whose contour is nonlinear, where the nonlinearity is due to the presence of radiation in the system. The Bayesian method used in the inverse problems is based on the particle filter Sampling Importance Re-sampling (SIR), which is combined with the MFS to enable the estimation of the temperature field, while a random walk performs the estimation of the heat transfer coefficient (HTC) simultaneously. The results of the inverse problems were satisfactory for the linear boundary problems, while the nonlinear contour problems were most computational costly, despite their high accuracy.

Keywords: Method of Fundamental Solutions, Parabolic Problems, Bayesian Methods, State and Parameter Estimation, Particle Filter, SIR.

LIST OF FIGURES

LIST OF TABLES

LIST OF CONTENTS

ABBREVIATION LIST

BEM
Boundary Element Method, 15, 16, 17, 51, 54
BKM
Boundary Knot Method, 15
DRM
Dual Reciprocity Method, 18, 67
FDM
Finite Difference Method, 15, 19, 20
FVM
Finite Volume Method, 15
HTC
Heat Transfer Coefficient, vi, 15, 16, 17, 18, 27, 28, 29, 30, 32, 33, 37, 38, 41, 46, 51, 54, 55, 60, 64, 67
IHCP
Inverse Heat Conduction Problem, 20
IRM
Iterative Regularization Method, 15
KF
Kalman Filter, 16
MCMC
Markov Chain Monte Carlo, 16, 51
MFS
Method of Fundamental Solutions, vi, 15, 16, 17, 18, 19, 20, 21, 24, 25, 27, 29, 38, 39, 40, 41, 43, 44, 45, 51, 52, 54, 56, 57, 58, 61, 62, 63, 66, 67
MFS-D
Method of Fundamental Solutions Dual, 18
MPS
Method of Particular Solutions, 19
PDE
Partial Differential Equation, 16
PDEs
Partial Differential Equations, 18
RBF
Radial Basis Function, 18, 19
Rel
Relative Error, 41, 51
RMSE
Root-mean Squared Error, 41
SIR
Sequential Importance Resampling, vi, 16, 17, 37, 38, 39, 42, 46, 47, 48, 49, 53, 59, 63, 67
SIS
Sequential Importance Sampling, 16, 38, 39
SVD
Singular Value Decomposition, 19, 44, 57
TMMFS
Time Marching Method of Fundamental Solutions, 19, 20

LIST OF SYMBOLS

$\boldsymbol{a}$	- Generic event 1
A	- Fundamental solutions matrix
$\tilde{A}$	- Fundamental solutions matrix augmented with standard or non standard measurements data
$\boldsymbol{b}$	- Generic event 2
$\mathcal{B}$	- Boundary operator
$\boldsymbol{B}$	- Column vector of given information
$\widetilde{\boldsymbol{B}}$	- Column vector of given information augmented with standard/non standard measurements information
$\boldsymbol{c}$	- Unknown coefficients
c_λ	- Regularized unknown coefficients
CP	- Number of collocation points
d	- Distance between boundary and source points fictious domain
E	- Nonstandard measurements
$\boldsymbol{f}_{k-1}$	- Evolution model
F	- Fundamental Solution
h	- Third kind boundary data
$\boldsymbol{h}_k$	- Observation model
H	- Heaviside function
I	- Identity matrix
$\mathcal{L}$	- Linear Differential Operator
M	- Time-points from MFS discretization process
n	- Spatial dimension
$\boldsymbol{n}_k$	- Measurement noise/unverainty vector
N	- Spatial-points from MFS discretization process
ND	- Number of points inside the study domain
NS	- Number of source points
N_{part}	- Number of particles from particle filter
p	- Percentage of noise
P	- Dirichlet data

$\boldsymbol{P}_k$ - State vector at given timestep k

Q - Neumann data

t - Time coordinates from the study domain

t_{final} - Last time in the study domain

T - Temperature

T^0 - Temperature at instant $t = 0$

u - Unknown function

u_N - Unknown function approximation

u_0 - Unknown function at $t = 0$

$\boldsymbol{v}_{k-1}$ - Unverainty vector from model

$\boldsymbol{x}$ - Spatial coordinates from collocation points

$\boldsymbol{y}$ - Spatial coordinates from source points

Y - Standard measurements

$\boldsymbol{z}_k$ - Measurements given the target state

$\boldsymbol{Z}_k$ - Available measurements at time k

GREEK SYMBOLS

α - Diffusivity

γ_k - Random values drawn from a uniform distribution

δ - Dirac's delta

ζ - Random value drawn from a normal distribution with zero mean and known standard deviation

ε_k - Random values draw from a Gaussian distribution

λ - Regularization parameter from Tikhonov

$\boldsymbol{\nu}$ - Outward unit normal

ρ - Heat transfer coefficient

σ - Standard deviation from measurements

σ_ρ - Standard deviation representing the random walk from HTC evolution model

τ - Time coordinates from the source points

$\Phi(T)$ - Primitive of $g(T)$

Ω - Domain

$\partial\Omega$ - Domain's boundary

1 INTRODUCTION

The heat transfer coefficient (HTC) characterizes the contribution that an interface makes to the overall thermal resistance to the system and is defined in terms of the heat flux across the surface for a unit temperature gradient ([1], [2]). As an important parameter of the thermal system, the estimation of the HTC is a common task. Some non-intrusive experimental techniques as one based on characteristic colour changes of liquid crystal films at a given temperature or on laser-induced fluorescence rely on the one-dimensional analytical temperature solution for a semi-infinite medium to determine the HTC at a point once the temperature history is obtained from the experiment, thus this method is difficult to use in a truly time-dependent process where the HTC varies as a function of time [2].

In respect to time-dependent HTC, a work in [3] addresses the estimation of the time and space dependent HTC during the “Jominy end Quench”. The numerical study uses the Iterative Regularization Method (IRM) and the Function Specification Method (FSM). The estimation of the HTC during the “Jominy end-Quench” is highly nonlinear principally in the thermal conductivity during the phase transformations (austenite–martensite). Some strategies for the inverse problem of reconstruction of the HTC are given in [4], [5], and [6]. Traditionally, partial boundary temperature and heat flux measurements are used as input to heat conduction models to extract the HTC values by solving a Cauchy ill-posed inverse heat conduction problem, but in cases that the obtainment of Cauchy data is difficult or impossible, non-standard measurements can be used [2].

In general, when an inverse transient heat problem is solved iteratively, it’s necessary to use a direct problem solver that is fast and accurate, what has turned attention to meshless methods. Meshless methods recently gained attention in science and engineering problems as a competitive alternative to mesh-dependent numerical schemes, as finite difference method (FDM) and finite volume method (FVM), that require a mesh on the domain to support the solution process. A mesh generation can be extremely time-consuming to well-behaved mesh for complicated geometry in higher dimensions. As alternative, boundary-based methods as the most famous one boundary-elements method (BEM) reduces the dimensionality of the problem by one, but requires an evaluation of singular integrals for using singular fundamental solutions [7]. Some notable meshless methods are the Kansa’s method, [8], the boundary knot method (BKM), [9], and the method of fundamental solutions (MFS).

The MFS is a meshless, integration free, easy to implement, and powerful method that have gained more attention in the context of meshless methods. Unlike the BEM, the MFS does not require the evaluation of singular integrals. This MFS simplicity and accuracy make it an interesting method to be applied in schemes to solve inverse problems.

For inverse problems in the Bayesian framework, state estimation problems are often solved with the so-called Bayesian filter, which requires relatively low computational demands compared to the Markov Chain Monte Carlo (MCMC) algorithm [10]. The most widely known Bayesian filter is the Kalman Filter (KF) [11] which is, however, limited to linear models with additive Gaussian noise. Some extension of KF are less restricted and being applied to non-linear problems, but it suffers from lack of theoretical rigor.

Sequential Monte Carlo methods, the so-called particle filters, have been developed in order to represent the *posteriori* density in terms of random samples and associated weights, and can be applied to non-linear systems with non-Gaussian errors ([12], [13], [14], and [15]).

In 1964, Hammersley & Hanscomb [16] presented a technique that uses recursive Bayesian filters along with Monte Carlo simulations, a so-called sequential importance sampling (SIS). The key idea is to represent the *posteriori* probability function as a set of random samples with associated weights to estimate the state. An extra step, named resampling, was implemented in the SIS algorithm for Gordon *et al.* [17] in order to attenuate the particle degeneration process resulting of the importance sampling., in a filter known as sequential importance re-sampling (SIR).

A comparison of particle filter SIR and Kalman filter to estimate the transient temperature field in two different heat conduction problems is made in [18], one linear, and other non-linear. On the linear case, the methods provide results of similar accuracy. The Kalman filter approach is not valid for non-linear and/or non-Gaussian models. The particle filter SIR shows more robustness, being applied to a wider range of problems, and present a high computational cost related to the Kalman filter.

This present work aims to investigate the MFS coupled with the particle filter SIR (MFS-PF) in order to estimate the time-dependent heat transfer coefficient (HTC) in the parabolic heat conduction PDE for one and two-dimensional problems with convective and radiative boundary conditions. All numerical procedure was using the MATLAB program. The CPU specifications are defined in numerical results (session 6).

The estimation of the HTC using the MFS-PF uses different kinds of measurements (see in 3.1 and 3.2), including the measurement on non-standard boundary transient quantity of the heat conducting system, allowing the prescription of convectional boundary conditions over the whole boundary, like described in [1], where the BEM is used to estimate the time-dependent HTC. This approach make it possible to propose more realistic models for the estimation of the transient HTC, since the real problems deals with variations in many factors [19] such as velocity of the fluid, fluid properties (viscosity, density, and thermal conductivity), and orientation of the flow.

In session 2, a general mathematical formulation of the MFS is described for a generic operator and for parabolic problems. A brief review of MFS and its main characteristics are presented.

In session 3, the MFS is investigated to solve direct parabolic problems with third kind boundary conditions. The source points and collocation points are defined.

In session 4, the formulation of the inverse problem from this present work is described for one and two spatial dimensions.

In session 5, the Bayesian methods are presented, with special attention to the particle filter SIR, that is used in the HTC estimation problem. A pseudo-code for the SIR is shown.

In session 6, all numerical results are shown. Two problems involving linear boundary and other two problems with nonlinear boundary conditions are solved.

In session 7, a general discussion about the MFS-PF is made, and some future works are suggested.

The references from this present work are shown in session 8.

2 THE METHOD OF FUNDAMENTAL SOLUTIONS

The method of fundamental solutions (MFS) is a relatively old, and recently have gained attention to solve parabolic problems. In this session, a brief introduction to the MFS is presented in order to contextualize the evolution of the method in parabolic and inverse problems, and its main advantages and disadvantages. Furthermore, a general mathematical formulation of the method, and its approach to solve the one-dimensional and two-dimensional transient HTC problem is shown.

2.1 A BRIEF INTRODUCTION TO THE MFS

The method of fundamental solutions (MFS) was initially proposed by Kupradze & Aleksidze in 1964 [20], having a numerical implementation discussed by Mathon & Jhonston in 1977 [21], where two-dimensional elliptic Dirichlet problems were solved by using fundamental solutions with singularities placed outside the region of interest. The method presented accurate and relatively uniform approximations. The singularities coordinates were chosen by a nonlinear least square algorithm to make the method more flexible. In 1985, Bogomolny [22] presented denseness results from MFS applied to elliptic problems with sources, or singularities, located outside the solution domain.

Since the denseness results are mainly valid for elliptic partial differential equations (PDEs), other works involving the Laplace, modified Helmholtz or biharmonic PDEs was widely developed. In respect to non-homogeneous problems, the MFS cannot be used in standard form. Some methods uses solutions of the Helmholtz equation to approximate the source terms, like in [23] and [24], where a Poisson problem is solved using the so-called MFS-D. A dual-potential formulation in [25] uses the MFS for Laplace and biharmonic equations to solve multidimensional Stokes equation resulting in a simple implementation method with good accuracy. The main concept of this methods is based on the evaluation of a particular solution using the dual reciprocity method (DRM) [26] and radial basis functions (RBF) [27]. In this present work all the cases are homogeneous.

The method simplicity and accurate results with simple codes and small computational effort promoted the development of hybrid methods in order to extend the MFS to parabolic and hyperbolic PDEs using a time-marching process to advance the solution in the time domain.

A time-marching scheme using the method of fundamental solutions (TMMFS) is proposed in [28] to solve transient heat conduction problems for materials with non-constant properties. In this approach, the transient equation is transformed into a sequence of inhomogeneous Helmholtz-type equations, where the time derivative of the solution is approximating through a FDM scheme, and the elliptic boundary value problem is solved by MFS using the Helmholtz fundamental solution, where resulting system is solved from each time step by a singular value decomposition (SVD) solver. This hybrid method presented stable and accurate results.

This approach is extended for wave equations in [29], where the hyperbolic equation can be viewed as a Poisson-type equation with time-dependent source term, that is solved with a Houbolt FDM scheme. The particular solution is approximated by radial basis function (RBF) in a method of particular solution (MPS) scheme. Similar approach is used in in [30] to more general problems, solving multi-dimensional Telegraph Equations and presenting good efficiency and accuracy.

The TMMFS scheme have a time-discretization necessity what avoid the main characteristic of meshless methods. Furthermore, the procedure of transform parabolic or hyperbolic equations in elliptic expressions, like Laplace or Poisson, can be not so trivial.

In order to propose a method free from Laplace transform or time-marching scheme using FDM, Young *et al.* [31] use the time-dependent fundamental solution of the diffusion equation directly to approximate the solution as a linear combination of the fundamental solution of diffusion operator in homogeneous problems. The source points are placed outside the time-domain. This approach is compared to TMMFS in [32], resulting in worst results than using Laplace transformation.

Other approach of MFS applied to transient heat conduction problems is investigated by Johansson & Lesnic [33], where the source-points are placed outside the space domain, as is done in stationary case, to guarantee the denseness results already proved in [22] and as suggested by Kupradze [20]. This approach is compared to the case of the source points placement outside the time-domain, reaching more accurate results for Dirichlet problems. Furthermore, this paper shows that when the source-points are placed too close to domain boundary the approximation is less accurate. Same occurs when these source points are placed at a too large distance.

An extension of the method from [33] is investigated in [34] to layered materials with a technique in which the source points were located outside the boundary of the space solution domain for each layer. The results shown a good agreement with the analytical solutions for some two- and three-layered materials.

A study in [35] shows a comparison about the three different approaches to solve a transient heat conduction problem in a 2D unit square domain using Dirichlet and Neumann boundary data. The three different versions of MFS consist in the MFS with Laplace transformation of the governing differential equations and boundary conditions, the second is the MFS with time-dependent fundamental solution, and third, the TMMFS scheme using backward difference scheme. For all these methods, the temperature can be computed in a whole domain, and all versions give acceptable results with respect to the root mean squared relative error. In general way, the TMMFS scheme can obtain the best results, being the simplest for studied cases. Related to computational cost, the TMMFS represents the most computational costly, and the MFS with Laplace transformation, the lowest cost.

A work about the MFS to solve two-dimensional heat conduction problems is given in [36], where the 2D heat conduction problems denseness results are proved. Direct problems are discussed, varying the configuration of the source points in a square shape and a circle. The examples shown lower dependency of the source points placement in relation to 1D cases. Furthermore, an inverse problem with overspecified boundary is solved. Linear Dirichlet problems are solved with accurate approximation at small computational cost. An analysis varying the diffusivity is made and presents good results. Same authors proposed an application of the MFS to the radially symmetric inverse heat conduction problem (IHCP) in [37], having a stable and accurate numerical approximation with small computational cost. In this approach, the fundamental solution of the radially symmetric heat equation is used, and a Cauchy problem is solved.

A major drawback from MFS is the source points placement dependence in relation of approximated solutions accuracy [38], in this context, an investigation about the source points placement in parabolic problems was recently proposed in [39] and [40]. In this papers, various source points placement strategies are compared in relation with the accuracy of the approximated solution. A discussion is held about the use of term “pseudo-boundary” in initial-boundary value problems, instead of this term is strictly related to the original idea of solving boundary value problems.

Related to inverse problems, the MFS was found to be an efficient and accurate method. The resulting system of linear algebraic equations from MFS are naturally ill-conditioned, what is a disadvantage to any well-known numerical methods such as FDM or other boundary based methods, while the MFS's advantages are preserved, such as its simple implementation and its ease of application in irregular domains [41].

Some main advantages and disadvantages are highlight by [42]:

Advantages:

- The method is relatively easy to program and computationally inexpensive;
- The MFS is a collocation method, therefore no complicated meshes need to be generated;
- It has produced accurate and stable results for different types of problems (elliptic, parabolic, free boundary, etc.).

Disadvantages:

- The MFS can only be applied when the fundamental solution of the governing linear PDE is known.
- The position and number of source and collocation points can affect the accuracy greatly, it is possible to solve a nonlinear minimization problem to determine the position of the source points, however, this can significantly increase the computational time.

In this present work, the MFS is applied in the context of time-dependent fundamental solutions, using one e two-dimensional formulation that the denseness results are well known. The mathematical formulation is described for the direct problem in session 3, and for the inverse problem in session 4.

2.2 GENERAL MATHEMATICAL FORMULATION

Consider a bounded domain Ω

$$\mathcal{L}(u) = 0, \tag{2.1}$$

where $\mathcal{L}$ is a linear differential operator with constant coefficients and $u: \mathbb{R}^n \to \mathbb{R}$. The data given on the boundary $\partial\Omega$ can be rewriten as

$$\mathcal{B}u(\boldsymbol{x}) = f(\boldsymbol{x}), \tag{2.2}$$

where $f(x) : \mathbb{R}^n \to \mathbb{R}$. The fundamental solution $F(x, y)$ of equation eq.(2.1) satisfies

$$\mathcal{L}(F) = \delta(\boldsymbol{x}, \boldsymbol{y}), \tag{2.3}$$

where δ is the Dirac delta function, and $\boldsymbol{y}$ is the coordinate of a source point, placed outside the study domain Ω. The generalized Dirac delta distribution function is given by

$$\delta(\boldsymbol{x}, \boldsymbol{y}) = \delta(\boldsymbol{x} - \boldsymbol{y}) = \begin{cases} \infty, & \boldsymbol{x} = \boldsymbol{y} \\ 0, & \boldsymbol{x} \neq \boldsymbol{y} \end{cases}, \tag{2.4}$$

with

$$\int_{\mathbb{R}^n} \delta(\boldsymbol{x} - \boldsymbol{y})\, d\boldsymbol{x} = 1. \tag{2.5}$$

Considering a function $f(\,)$, the fundamental Dirac delta distribution are given by

$$\int_{\Omega} f(\boldsymbol{y})\delta(\boldsymbol{x}, \boldsymbol{y})\, d\boldsymbol{y} = f(\boldsymbol{x}), \quad \boldsymbol{x} \in \Omega. \tag{2.6}$$

The functions are essentially nonzero only in a neighborhood of their boundary points [21], and the optimal distance between this points need to be investigated or determinated by a nonlinear optimization process. Once $\boldsymbol{y}$ is placed outside the region where the solution is sought, the fundamental solution $F(\boldsymbol{x}, \boldsymbol{y})$ and any linear combination of fundamental solutions satisfies the eq.(2.1). This way, with known $\boldsymbol{x}$ and $\boldsymbol{y}$ position, we can define an approximation to eq.(2.2) in the form

$$u_N(\boldsymbol{x}) \cong \sum_{j=1}^{NS} c_j F(\boldsymbol{x}, \boldsymbol{y}_j), \tag{2.7}$$

where y_j represent NS source points placed outside the domain Ω, and $u_N(\boldsymbol{x})$ represents well known points placed on the boundary, here in this work given by collocation. The c_j component refers to unknown coefficients. The **Figure 1** shows a possible configuration of a generic domain Ω and $CP = 9$ collocation points on boundary and $NS = 9$ source points outside Ω.

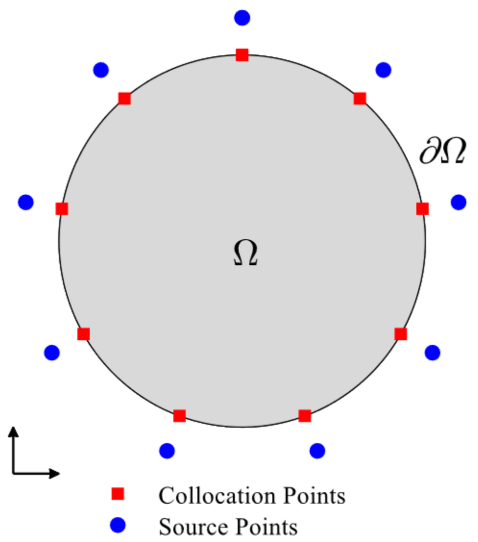

Figure 1 – Possible source points and collocation points placement in a generic circular domain.

Some fundamental solutions for linear differential operators are given in **Table 1**.

Table 1 – Some fundamentals solutions for elliptic operators.

OPERATOR		$\boldsymbol{n}$	$\boldsymbol{F}(\boldsymbol{x}, \boldsymbol{y})$
Laplace	$\Delta u(\boldsymbol{x}) = 0$	$\mathbb{R}^2$	$\frac{1}{2\pi}\log\|\boldsymbol{x}-\boldsymbol{y}\|$
		$\mathbb{R}^3$	$-\frac{1}{4\pi}\frac{1}{\|\boldsymbol{x}-\boldsymbol{y}\|}$
Helmholtz	$(\Delta + \xi^2)u(\boldsymbol{x}) = 0$	$\mathbb{R}^2$	$-\frac{1}{4}H_0^{(2)}(\xi\|\boldsymbol{x}-\boldsymbol{y}\|)$
		$\mathbb{R}^3$	$-\frac{1}{4}H_0^{(2)}(\xi\|\boldsymbol{x}-\boldsymbol{y}\|)$
Modified Helmholtz	$(\Delta - \xi^2)u(\boldsymbol{x}) = 0$	$\mathbb{R}^2$	$\frac{1}{2\pi}K_0(\xi\|\boldsymbol{x}-\boldsymbol{y}\|)$
		$\mathbb{R}^3$	$\frac{1}{4\pi\|\boldsymbol{x}-\boldsymbol{y}\|}exp(-\xi\|\boldsymbol{x}-\boldsymbol{y}\|)$

*ξ reffers to the eigenvalue (or wave number in the study of waves)

In this present work, the governing equation is the parabolic heat equation. To better understand the MFS in this context, consider the parabolic heat equation:

$$\frac{\partial u}{\partial \mathrm{t}}(\boldsymbol{x},t) = \alpha^2 \frac{\partial u^2}{\partial \boldsymbol{x}^2}(\boldsymbol{x},t)\,, \qquad \boldsymbol{x} \in \Omega, \qquad t \in \left(0, t_{final}\right], \tag{2.8}$$

where $\Gamma_1 \cup \Gamma_2 = \partial\Omega$, Γ_1 represents Dirichlet data, Γ_2 represents Neumann data. The α term corresponds to the diffusivity of medium, $u(\boldsymbol{x},t) = T(\boldsymbol{x},t)$ is the temperature. In these problems we need to know domain data in a given time in ND different points. For simplicity, we assume that information about domain is known when $t = 0$. We can describe the initial condition as

$$u(\boldsymbol{x},0) = u_0(\boldsymbol{x}), \qquad \boldsymbol{x} \in \Omega = (0,1), \tag{2.9}$$

and boundary conditions

$$u(\boldsymbol{x},t) = P(\boldsymbol{x},t), \qquad \boldsymbol{x} \in \Gamma_1, \qquad t \in \left(0, t_{final}\right], \tag{2.10}$$

$$\frac{\partial u}{\partial \nu}(\boldsymbol{x},t) = Q(\boldsymbol{x},t), \qquad \boldsymbol{x} \in \Gamma_2, \qquad t \in \left(0, t_{final}\right], \tag{2.11}$$

where ν is the outer unit normal with respect to the respective boundary. As in eq.(2.7), we can approximate the boundary data as a sum of fundamental solutions. The fundamental solution of eq.(2.8) is defined in terms of the diffusivity, the colocation points coordinates $(\boldsymbol{x},t)$ and the source points coordinates $(\boldsymbol{y},\tau)$, as,

$$F(\boldsymbol{x},t;\boldsymbol{y},\tau) = \frac{H(t-\tau)}{\left(4\pi\alpha^2(t-\tau)\right)^{\frac{n}{2}}}\; e^{-\frac{(\boldsymbol{x}-\boldsymbol{y})^2}{4\alpha^2(t-\tau)}}, \tag{2.12}$$

where n represents the spatial dimension number, and H represents the Heaviside function, which is introduced to emphasize that the fundamental solution is zero for $t < \tau$ [31]. The domain in eq.(2.9) and boundaries eq.(2.10) and eq.(2.11) can be approximated using MFS as, respectively, [39]:

$$\sum_{j=1}^{NS} c_j F(\boldsymbol{x_i}, t_i; \boldsymbol{y}_j, \tau_j) = u_0(\boldsymbol{x}_i), \qquad \boldsymbol{x}_i \in \Omega, \qquad i = 1,2,\dots,ND, \tag{2.13}$$

$$\sum_{j=1}^{NS} c_j F(\boldsymbol{x_i}, t_i; \boldsymbol{y}_j, \tau_j) = P(\boldsymbol{x}_i, t_i), \qquad \boldsymbol{x_i} \in \Gamma_1, \qquad i = 1,2,\dots,NC(\Gamma_1), \tag{2.14}$$

$$\sum_{j=1}^{NS} c_j \frac{\partial F}{\partial \nu}(\boldsymbol{x_i}, t_i; \boldsymbol{y}_j, \tau_j) = Q(\boldsymbol{x}_i, t_i), \qquad \boldsymbol{x}_i \in \Gamma_2, \qquad i = 1,2,\dots,NC(\Gamma_2), \tag{2.15}$$

where $t \in (0, t_{final}]$. Once $D(\boldsymbol{x}_i, t_i)$ and $Q(\boldsymbol{x}_i, t_i)$ are known for all NC collocation points, we can determine the unknown coefficients $\boldsymbol{c}$ solving

$$\begin{bmatrix} F(x_1, 0, y_1, \tau_1) & \cdots & F(x_1, 0, y_{NS}, \tau_{NS}) \\ \vdots & \cdots & \vdots \\ F(x_{ND}, 0, y_1, \tau_1) & \cdots & F(x_{ND}, 0, y_{NS}, \tau_{NS}) \\ F\left(x_{1(\Gamma_1)}, t_{1(\Gamma_1)}, y_1, \tau_1\right) & \cdots & F\left(x_{1(\Gamma_1)}, t_{1(\Gamma_1)}, y_{NS}, \tau_{NS}\right) \\ \vdots & \cdots & \vdots \\ F\left(x_{NC(\Gamma_1)}, t_{NC(\Gamma_1)}, y_1, \tau_1\right) & \cdots & F\left(x_{NC(\Gamma_1)}, t_{NC(\Gamma_1)}, y_{NS}, \tau_{NS}\right) \\ F\left(x_{1(\Gamma_2)}, t_{1(\Gamma_2)}, y_1, \tau_1\right) & \cdots & F\left(x_{1(\Gamma_2)}, t_{1(\Gamma_2)}, y_{NS}, \tau_{NS}\right) \\ \vdots & \cdots & \vdots \\ F\left(x_{NC(\Gamma_2)}, t_{NC(\Gamma_2)}, y_1, \tau_1\right) & \cdots & F\left(x_{NC(\Gamma_2)}, t_{NC(\Gamma_2)}, y_{NS}, \tau_{NS}\right) \end{bmatrix} \begin{bmatrix} c_1 \\ \vdots \\ \vdots \\ \vdots \\ \vdots \\ \vdots \\ \vdots \\ \vdots \\ c_{NS} \end{bmatrix} = \begin{bmatrix} u_0(x_1) \\ \vdots \\ u_0(x_{ND}) \\ P(x_{1(\Gamma_1)}, t_{1(\Gamma_1)}) \\ \vdots \\ P(x_{NC(\Gamma_1)}, t_{NC(\Gamma_1)}) \\ Q(x_{1(\Gamma_2)}, t_{1(\Gamma_2)}) \\ \vdots \\ Q(x_{NC(\Gamma_2)}, t_{NC(\Gamma_2)}) \end{bmatrix} \tag{2.16}$$

The expression from eq.(2.16) can be written in a generic form as

$$A\boldsymbol{c} = \boldsymbol{B}, \tag{2.17}$$

where A is the fundamental solution matrix with $ND + NC(\Gamma_1) + NC(\Gamma_2)$ rows and NS columns, c is a column of NS elements, that contains all unknown coefficients and $\boldsymbol{B}$ is the column with $ND + NC(\Gamma_1) + NC(\Gamma_2)$ elements, given by the initial-boundary information. With $\boldsymbol{c}$, we can approximate every point of study domain Ω and t as in eq.(2.7).

A well-known issue with the MFS is that the resulting system of equations is ill-conditioned and a straightforward inversion will produce unstable results. When $g(T) = T$, as in the Newton's law of cooling, the resulting system is linear. In order to stabilize the solution, it is usual to apply the Tikhonov regularization method and solve

$$\min_c\{\|A(\boldsymbol{c})-\boldsymbol{B}\|^2+\lambda\|\boldsymbol{c}\|^2\}, \tag{2.18}$$

where $\lambda \geq 0$ is a regularization parameter to be prescribed. The minimization problem can be solved exactly to yield the regularized solution:

$$\boldsymbol{c}_\lambda = (A^TA+\lambda I)^{-1}A^T\boldsymbol{B}, \tag{2.19}$$

where ^{T} denotes the transpose of a matrix and I is the identity matrix. A common method to choose λ is the L-curve ([41], [43]), where is varying λ and the vertical axis is given by $log\|\boldsymbol{c}\|$ and the horizontal axis is given by the residual given by $log\|A\boldsymbol{c}-\boldsymbol{B}\|$. The resulting L-shape indicates that the λ near to the corner is a reasonable choice (see session 6.1.1 and 6.2.1).

3 DIRECT PROBLEM FORMULATION

For the direct problem, consider the parabolic heat conduction governing equation (eq.(2.8)) with third kind boundary conditions, initial conditions, and known HTC. The approach for the one-dimensional and multidimensional problems are given in the next sessions. Considering the thermal diffusivity $\alpha = 1$, whilst the heat source is assumed to be absent, and $u(x,t) = T(x,t)$.

3.1 ONE-DIMENSIONAL MFS

Considering a one-dimensional finite slab $\Omega \subset [0,1]$ governed by the parabolic heat equation from eq.(2.8), that satisfy:

$$\frac{\partial T}{\partial \mathrm{t}}(x,t) = \frac{\partial^2 T}{\partial x^2}(x,t), \qquad (x,t) \in \Omega \times (0,t_f), \tag{3.1}$$

$$T(x,0) = T^0(x), \qquad x \in (0,1), \tag{3.2}$$

$$-\frac{\partial T}{\partial x}(0,t) + \rho(t) g\big(T(0,t)\big) = h_0, \qquad t \in \big[0,t_f\big), \tag{3.3}$$

$$\frac{\partial T}{\partial x}(1,t) + \rho(t) g\big(T(1,t)\big) = h_1, \qquad t \in \big[0,t_f\big), \tag{3.4}$$

where g, T^0, h_0 and h_1 are given functions. Assuming the one-dimensional fundamental solution, the expression in eq.(2.12) is given by

$$\mathrm{F}(x,t;y,\tau) = \frac{H(t-\tau)}{\sqrt{4\pi(t-\tau)}}\; e^{-\frac{(x-y)^2}{4(t-\tau)}}, \tag{3.5}$$

where eq.(3.5) needs to be derived in the space in order to solve Neuman or mixed boundaries:

$$\frac{\partial \mathrm{F}}{\partial \mathrm{x}}(x,t;y,\tau) = \frac{(y-x)H(t-\tau)}{4\sqrt{\pi(t-\tau)^3}}\ e^{-\frac{(x-y)^2}{4(t-\tau)}}. \tag{3.6}$$

Then, the approximate solution for one-dimensional cases can be sought as in [33] and [39],

$$T_M(x,t) = \sum_{m=-M+1}^{M} c_m^{(0)} F(x,t;y_0,\tau_m) + \sum_{m=-M+1}^{M} c_m^{(1)} F(x,t;y_1,\tau_m)\,, \quad (x,t) \in \Omega \times [0,t_f]\,, \tag{3.7}$$

where the timed-source points are given by

$$\tau_m = \frac{2m-1}{2M} t_f, \qquad m = -M+1, \dots, M, \tag{3.8}$$

and the spatial-source points are

$$y_0 = -d;\ y_1 = 1+d, \qquad d > 0\,, \tag{3.9}$$

where d is the distance from the source points to the boundary, and M represents the truncation level of an infinite series expansion whose span is dense in the set of functions satisfying the heat equation eq.(2.8). In the direct problem eq.(3.1)-(3.4), the HTC $\rho(t)$ is known and only the coefficients $c_m^{(0)}$ and $c_m^{(1)}$ for $m = -M+1, \dots, M$ are unknown and have to be determined by imposing the initial and boundary conditions eq.(3.2)-(3.4).

Selecting the time points from study domain $t_k = \frac{kt_f}{M}$, with $k = 0, \dots, M$ and the spatial domain points $x_l = \frac{l}{N+1}$ for $l = 1, \dots, N$, we obtain a system of $(N + 2M + 2)$ equations with $4M$ unknowns. Given the approximation of initial and boundary conditions, respectively:

$$\sum_{\mathrm{i}=0}^{1} \sum_{\mathrm{m}=-\mathrm{M}+1}^{\mathrm{M}} c_m^{(i)} F(x_l,0;y_i,\tau_m) = T^0(x_l), \qquad l = 1, \dots, N, \tag{3.10}$$

$$-\sum_{i=0}^{1}\sum_{m=-M+1}^{M} c_m^{(i)} \frac{\partial F}{\partial x}(0,t;y_i,\tau_m) + \rho_k g\left(-\sum_{i=0}^{1}\sum_{m=-M+1}^{M} c_m^{(i)} F(0,t;y_i,\tau_m)\right) = h_0(t_k),$$
$$k = 0, \dots, M, \tag{3.11}$$

$$\sum_{i=0}^{1}\sum_{m=-M+1}^{M} c_m^{(i)} \frac{\partial F}{\partial x}(1,t;y_i,\tau_m) + \rho_k g\left(-\sum_{i=0}^{1}\sum_{m=-M+1}^{M} c_m^{(i)} F(1,t;y_i,\tau_m)\right) = h_1(t_k),$$
$$k = 0, \dots, M, \tag{3.12}$$

where $\rho_k = \rho(t_k)$. The above system can be written in a generic form $A\boldsymbol{c} = \boldsymbol{B}$, where $\boldsymbol{c}$ is the vector of unknowns, $\boldsymbol{B}$ is the initial and boundary values given and A is the matrix of fundamental solutions.

Once the boundary data is convective, therefore $g(T) = T$, the resultant system can be solved by a linear solver, like the SVD. The radiation boundary condition implying a nonlinearity in the resultant system, with $g(T) = T^3|T|$, and a nonlinear solver needs to be used.

3.2 MULTIDIMENSIONAL MFS

The formulation of the multidimensional problem is in two-dimensions, but essentially the same statements hold also in three-dimensions. Considering a two-dimensional bounded domain $\Omega \subset \mathbb{R}^2$ with sufficiently smooth boundary $\partial\Omega$

$$\frac{\partial T}{\partial \mathrm{t}}(x_1,x_2,t) = \frac{\partial^2 T}{\partial x_1^2}(x_1,x_2,t) + \frac{\partial^2 T}{\partial x_2^2}(x_1,x_2,t), \qquad (x_1,x_2,t) \in \Omega \times (0,t_f), \tag{3.13}$$

$$T(x_1,x_2,0) = T^0(x_1,x_2), \qquad x \in \Omega, \tag{3.14}$$

$$\frac{\partial T}{\partial \boldsymbol{\nu}}(x_1,x_2,t) + \rho(t) g\big(T(x_1,x_2,t)\big) = h(x_1,x_2,t), \qquad t \in \partial\Omega \times \big[0,t_f\big), \tag{3.15}$$

where $\boldsymbol{\nu}$ is the outward unit normal to the boundary $\partial\Omega$, g, T^0 and h are given functions.

Assuming the two-dimensional fundamental solution, the expression from eq.(2.12) is given by

$$\mathrm{F}(\boldsymbol{x}, t; \boldsymbol{y}, \tau) = \frac{H(t-\tau)}{4\pi(t-\tau)}\, e^{-\frac{(\boldsymbol{x}-\boldsymbol{y})^2}{4(t-\tau)}}. \tag{3.16}$$

Then, the approximate solution for two-dimensional cases can be sought as in [36] and [39],

$$T_{M,N}(\boldsymbol{x}, t) = \sum_{m=1}^{2M} \sum_{j=1}^{N} c_m^{(j)} F\big(\boldsymbol{x}, t; \boldsymbol{y}_j, \tau_m\big), \qquad (x, t) \in \Omega \times [0, t_f]\,, \tag{3.17}$$

where the timed-source points are given by

$$\tau_m = \frac{2(m-M)-1}{2M} t_f, \qquad m = 1, \dots, 2M, \tag{3.18}$$

and, for simplicity, using polar coordinates to the spatial-source points:

$$y_j = \big(r_0 + d, \theta_j\big), \qquad \theta_j = \frac{2\pi j}{N}, \qquad j = 1, \dots, N, \qquad d > 0, \tag{3.19}$$

then, the eq.(3.17) can be rewritten, in polar coordinates, as

$$T_{M,N}(r, \theta, t) = \sum_{m=1}^{2M} \sum_{j=1}^{N} c_m^{(j)} F\big(r, \theta, t; r_0 + d, \theta_j, \tau_m\big), \tag{3.20}$$

where d is the distance from the source points to the boundary In the direct problem, eq.(3.13)-(3.15), the HTC $\rho(t)$ is known and only the coefficients $c_m^{(j)}$ for $m = 1, \dots, N$ are unknown and have to be determined by imposing the initial and boundary condition from eq.(3.14) and eq.(3.15).

Selecting the time-points $t_k = \frac{k t_f}{M}$, with $k = 0, \dots, M$ from study domain, and the spatial- points $r_l = r_0\sqrt{(l/M)}$ for $l = 1, \dots, M-1$, from domain, where the squareroot has been introduced to spread the points out within the domain, and not to cluster them at the center. Furthermore, we obtain a system of $\big(N(M-1)+N(M+1)\big) = 2NM$ equations with $2NM$ unknowns. Given the approximation of the initial and boundary conditions, respectively:

$$\sum_{m=1}^{2M}\sum_{j=1}^{N} c_m^{(j)} F\big(r_l,\theta_i,0;r_0+d,\theta_j,\tau_m\big) = T^0\big(r_l,\theta_j,0\big), \qquad l=1\dots,M-1,\;\; i=1,\dots,N, \tag{3.21}$$

$$\sum_{m=1}^{2M}\sum_{j=1}^{N} c_m^{(j)} \frac{\partial F}{\partial r}\,\big(r_0,\theta_i,t;r_0+d,\theta_j,\tau_m\big) + \rho_k g\left(\sum_{m=1}^{2M}\sum_{j=1}^{N} c_m^{(j)} F\,\big(r_0,\theta_i,t;r_0+d,\theta_j,\tau_m\big)\right) = h(r_0,\theta_i,t_k), \qquad i=1,\dots,N, \qquad k=0,\dots,M, \tag{3.22}$$

where $\rho_k = \rho(t_k)$. The above system can be written in a generic form $A\boldsymbol{c} = \boldsymbol{B}$, where $\boldsymbol{c}$ is the vector of unknowns, $\boldsymbol{B}$ is the initial and boundary values given and A is the matrix of fundamental solutions.

4 INVERSE PROBLEM FORMULATION

Considering the direct problem from session **3**, where all boundary data information is well known, the aim the direct problem is determining the temperature distribution $T(\boldsymbol{x},t)$. In this present work, the time-dependent HTC is consider missing, furthermore the aim of the inverse approach is to find the pair $\left(T(\boldsymbol{x},t),\rho(t)\right)$ given a final time of interest $t_f > 0$. Additional information for the missing HTC estimation is needed. The inverse problems in this present work are solved iteratively using bayesian approach in a MFS-PF scheme (see session **5**).

4.1 ONE-DIMENSIONAL CASE

In order to compensate the missing HTC, consider some additional information as suggested in [1], [2], and [44], the boundary temperature measurement

$$Y(t) = T(1,t), \qquad t \in \left[0, t_f\right), \tag{4.1}$$

or the nonlocal measurement

$$E(t) = \int_{\partial\Omega} \Phi(T(x,t)ds(x) = \Phi\big(T(0,t)\big) + \Phi\big(T(1,t)\big), \qquad t \in \partial\Omega \times \left[0, t_f\right), \tag{4.2}$$

where the $\Phi(T) = \int g(T)dT$ is a primitive of the function g governing the linear (e.g. convective $g(T) = T$) or nonlinear (e.g. radiative $g(T) = T^3|T|$) boundary heat transfer law [2].

As in the inverse problem the vector $\boldsymbol{\rho} = \left(\rho(t_k)\right)_{k=1,\dots,k_{final}}$ is unknown, where k_{final} refers to number of time-points of interest to estimate the HTC, the resultant system of equations need to be supplemented with additional measurements, that can be as in eq.(4.1) or eq.(4.2). With this, the system of equations from eq.(2.17) is extended to

$$\tilde{A}(\boldsymbol{c},\boldsymbol{\rho}) = \widetilde{\boldsymbol{B}}, \tag{4.3}$$

where $\widetilde{\boldsymbol{B}}$ is given by initial and boundary conditions given **B** along with $\left(E(t_k)\right)_{k=1,\dots,k_{final}}$ or $(\left(Y(t_k)\right)_{k=1,\dots,k_{final}}$, and $\tilde{A}$ is the extended matrix that contains the left-handed information of eq.(3.10), eq.(3.11) and eq.(3.12), along with eq.(4.1) or eq.(4.2). The Tikhonov regularization expression from eq.(2.18) with missing $\boldsymbol{\rho}$ is given by

$$\min_{\boldsymbol{c},\boldsymbol{\rho}} \left\{ \left\| \tilde{A}(\boldsymbol{c},\rho) - \widetilde{\boldsymbol{B}} \right\|^2 + \lambda(\|\boldsymbol{c}\|^2 + \|\boldsymbol{\rho}\|^2 \right\}. \tag{4.4}$$

4.2 MULTIDIMENSIONAL CASE

As in the inverse problem the vector $\boldsymbol{\rho} = \left(\rho(t_k)\right)_{k=1,\dots,k_{final}}$ is unknown, where k_{final} refers to number of time-points of interest. In order to compensate the missing time-dependent HTC, consider additional information given by non-local measurement, as in session 4.1:

$$E(t) = \int_{\partial\Omega} \Phi(T(x_1,x_2,t)ds(x_1,x_2)\,, \qquad t \in \partial\Omega \times \left[0,t_f\right), \tag{4.5}$$

where the $\Phi(T) = \int g(T)dT$ is a primitive of the function g governing the linear ($g(T) = T$) or nonlinear (e.g. radiative $g(T) = T^3|T|$) boundary heat transfer law [2]. As in direct problem, once the problem is axisymmetric, can be simplified using other coordinate systems. In polar coordinates, this non-standard measure is given as

$$E(t_k) = \int_0^{2\pi} \Phi(T(1,\theta,t))d\theta \cong \frac{2\pi}{N}\sum_{j=1}^{N} \Phi\left(T\left(1,\tilde{\theta}_j,t_k\right)\right), \qquad k = 1,\dots,M, \tag{4.6}$$

where $\tilde{\theta}_j = \frac{\pi(2j-1)}{N}$. Note that at the initial time $t = 0$, the initial condition from eq.(4.5) requires $E(0) = \int_0^{2\pi} \Phi(T(1,\theta,t))d\theta = 0$, so there is no need to impose the expression from eq.(4.6) for $k = 0$. With the data given by eq.(4.6), the system from eq.(2.17) is extended to

$$\tilde{A}(\boldsymbol{c},\boldsymbol{\rho}) = \widetilde{\boldsymbol{B}}, \tag{4.7}$$

where $\widetilde{\boldsymbol{B}}$ is given by initial and boundary conditions given **B** along with $\left(E(t_k)\right)_{k=1,\dots,k_{final}}$, and $\tilde{A}$ is the extended matrix that contains the left-handed information of eq.(3.21) and eq.(3.22), along with eq.(4.6). The Tikhonov regularization expression from eq.(2.18) with missing $\boldsymbol{\rho}$ is given by

$$\min_{\boldsymbol{c},\boldsymbol{\rho}} \left\{ \left\| \tilde{A}(\boldsymbol{c},\boldsymbol{\rho}) - \widetilde{\boldsymbol{B}} \right\|^2 + \lambda(\|\boldsymbol{c}\|^2 + \|\boldsymbol{\rho}\|^2 \right\}. \tag{4.8}$$

5 BAYESIAN METHODS

All procedure to solve inverse problems in this present work is based in the Bayesian framework. The term "Bayesian" is often used to describe the statistical inversion approach, which is based on the following principles [12]:

- All variables included in the model are modelled as random variables;
- The randomness describes the degree of information concerning their realizations;
- The degree of information concerning these values is coded in probability distributions;
- The solution of the inverse problem is the *posteriori* probability distribution, from which distribution point estimates and other statistics are computed.

In the Bayesian framework, the inverse problem can be expressed as in [12]: Given the data $\boldsymbol{b}$, find the conditional probability distribution $\pi(\boldsymbol{a}|\boldsymbol{b})$ of the variable $\boldsymbol{a}$. where $\pi(\boldsymbol{a}|\boldsymbol{b})$ denotes the conditional probability of $\boldsymbol{a}$ when $\boldsymbol{b}$ is given.

As the solution of the inverse problem within the Bayesian framework is tackled in the form of statistical inference of the *posteriori probability density*, based on the Bayes' theorem, described as

$$\pi(\boldsymbol{a}|\boldsymbol{b}) = \frac{\pi(\boldsymbol{b}|\boldsymbol{a})\pi_{prior}(\boldsymbol{a})}{\pi(\boldsymbol{b})}, \tag{5.1}$$

where $\pi(\boldsymbol{a}|\boldsymbol{b})$ is the *posteriori* probability density, which is the conditional probability distribution of the unknown parameter given the measurements, $\pi_{prior}(\boldsymbol{a})$ is the *priori* probability density, which is the model for the unknowns that reflects all the uncertainty of the parameters without the information conveyed by the measurements, $\pi(\boldsymbol{a}|\boldsymbol{b})$ is the likelihood function, which is the measurement model incorporating the related uncertainties, that is, the conditional probability of the measurements given the unknown parameters, and $\pi(\boldsymbol{b})$ is the marginal probability density of the measurements, which plays the role of a normalizing constant.

If the measurement errors are Gaussian random variables, with zero mean and known covariance matrix W, and the errors are additive and independent of the variables $\boldsymbol{a}$, the likelihood function can be expressed as

$$\pi(\boldsymbol{b}|\boldsymbol{a}) = (2\pi)^{-D/2} \exp\left\{-\frac{1}{2}[\boldsymbol{b} - T(\boldsymbol{a})]^{\boldsymbol{T}} W^{-1}[\boldsymbol{b} - T(\boldsymbol{a})]\right\}, \tag{5.2}$$

where D is the dimension of the observation vector. $T(\boldsymbol{a})$ represents the solution of the direct problem.

5.1 STATE ESTIMATION PROBLEM

The state estimation problem is a non-stationary inverse problem that is defined in the form of evolution and observation models, comprising stochastic processes. In nonlinear problems framework the particle filters offers in many cases better results than extensions of Kalman Filter, and its theoretical properties are becoming increasingly well-understood ([45], [46]).

In state estimation problems, the available measured data are used together with *priori* knowledge about the physical phenomena and the measuring devices, in order to sequentially produce estimates of the desired dynamic variables [47].

Consider a model for the evolution of the state variable

$$\boldsymbol{P}_k = f_{k-1}(\boldsymbol{P}_{k-1}, \boldsymbol{v}_{k-1}), \tag{5.3}$$

where f_{k-1} is, in general case, a nonlinear function of $\boldsymbol{P}$ and of the state noise/unverainty vector given by $\boldsymbol{v}_{k-1} \in \mathbb{R}^n$. The vector $\boldsymbol{P}_k \in \mathbb{R}^n$ is called state vector and contains the variables to be dynamically estimated. The eq.(5.3) is the state evolution model, and the subscript $k = 1, \dots, k_{final}$ denotes a time instant t_k in a dynamic problem.

The observation model describes the dependence between the state variable $\boldsymbol{P}_k$ to be estimated and the measurements $\boldsymbol{z_k}$ through the general function $\boldsymbol{h_k}$, that can be non-linear:

$$\boldsymbol{z}_k = \boldsymbol{h}_k(\boldsymbol{P}_k, \boldsymbol{n}_k), \tag{5.4}$$

where $\boldsymbol{n}_k$ represents the vector of measurement noise or uncertainty. This expression provides the solution of direct problem accounting for the state vector and the measurement uncertainty.

These models in eq.(5.3) and eq.(5.4) are based on the following assumptions ([12], [47]):

- The sequence $\boldsymbol{P}_k$ for $k = 1, \dots, k_{final}$ is a Markovian process, that is

$$\pi(\boldsymbol{P}_k|\boldsymbol{P}_1, \boldsymbol{P}_2, \dots, \boldsymbol{P}_{k-1}) = \pi(\boldsymbol{P}_k|\boldsymbol{P}_{k-1}), \tag{5.5}$$

- The same sequence $\boldsymbol{z}_k$ for $k = 1, \dots, k_{final}$ is a Markovian process with respect to the history of $\boldsymbol{P}_k$, that is,

$$\pi(\boldsymbol{z}_k|\boldsymbol{P}_1, \boldsymbol{P}_2, \dots, \boldsymbol{P}_k) = \pi(\mathbf{z}_k|\boldsymbol{P}_{k-1}), \tag{5.6}$$

- The sequence $\boldsymbol{P}_k$ depends on the past observations only through its own history, that is,

$$\pi(\boldsymbol{P}_k|\boldsymbol{P}_{k-1}, \mathbf{z}_1, \boldsymbol{P}_2, \dots, \mathbf{z}_{k-1}) = \pi(\boldsymbol{P}_k|\boldsymbol{P}_{k-1}), \tag{5.7}$$

Some strategies of Bayesian approach extends the state variable with the unknown parameters in order to estimate state and parameter at the same time ([48] and [49]). Other possibility is to use the particle filters, that rely on deterministic values of the model parameters. An option is applying the particle filter SIR by mimicking the parameters as state variables with an evolution model, for example, in the form of a random walk process. The parameters are then estimated sequentially along with the state variables. This approach can result in accurate estimation of parameters, even for physically complicated nonlinear problems such as in fire propagation [50].

The present work applies the SIR filter to the estimation of the temperature $T(\boldsymbol{x}, t)$ and the time-dependent HTC $\rho(t)$ from Robin boundary. Thus, the augmented state vector for one-dimensional problems (session 4.1) is given by

$$\boldsymbol{P}_k = \Big(\big(T(\boldsymbol{x}_l, t_k), \rho(t_k)\big)\Big), \qquad l = 1, \dots, N, \tag{5.8}$$

and, for multidimensional problem (session 4.2), the augmented state vector is defined as

$$\boldsymbol{P}_k = \Big(\big(T(r_l, \theta_j, t_k), \rho(t_k)\big)\Big), \qquad l = 1, \dots, M-1, \qquad j = 1, \dots, N, \tag{5.9}$$

The evolution model for the temperature is given by the MFS numerical approximation of direct problem while the evolution model for the HTC is a random walk.

$$\rho_k = \rho_{k-1} + \sigma_\rho \zeta_k, \qquad l = 1, \dots, N, \tag{5.10}$$

where ζ_k is a random value drawn from a normal distribution with zero mean and known standard deviation, and $\sigma_\rho = \sigma_\rho(k)$ is a positive constant to be prescribed at each timestep $(t_k)_{k=1,\dots,k_{final}}$. The models of evolution and observation used in this present work are shown in **Table 2**.

Table 2 – Models for the Bayesian procedure.

	One-dimensional	Multidimensional
Evolution Model – Temperature	$MFS(\boldsymbol{T}(\boldsymbol{x}_l, \boldsymbol{t}_{k-1}), \rho_k) + \boldsymbol{v}_k$	$MFS(T(\boldsymbol{r}_l, \boldsymbol{\theta}_j, \boldsymbol{t}_{k-1}), \rho_k) + \boldsymbol{v}_k$
Evolution Model - **HTC**	$\rho_k = \rho_{k-1} + \sigma_\rho \zeta_k$	$\rho_k = \rho_{k-1} + \sigma_\rho \zeta_k$
Observation Model	$\mathbf{z}_k = \boldsymbol{n}_k + T(1, t_k)$ or $\mathbf{z}_k = \boldsymbol{n}_k + E(t_k)$	$\boldsymbol{z}_k = \boldsymbol{n}_k + E(t_k)$

5.1.1 The Particle Filters

The particle filter is a Monte Carlo technique for the solution of state estimation problems, in which the *posteriori* density is represented by a set of particles with associated weights ([12], [47]). In the context of particle filters, the sequential importance sampling (SIS) is a method that estimates the *posteriori* distribution from a set of representative particles of the system variables [13], being a reference to many other last decade filters, and is an important reference to SIR, that is used in this present work.

The SIS consists in, for each step of time denoted as k, random samples are generated, the so-called particles, where each particle have a corresponding weight. The *priori* distribution provides the necessary information for the initial step, being the basis for the first particle draw. The likelihood function is then used to compare the initial information with the experimental measurements, and incorporates more information via particle weights in order to determine the *posteriori* distribution.

The SIS for the estimation problem follows the procedure described in [51]: For each $k = 1, \dots, k_{final}$: using the measured data $\boldsymbol{z}_k = \boldsymbol{z}(t_k)_{k=1,\dots,k_{final}}$, N_{part} particles for the states $\{\boldsymbol{P}_k^i\}_{i=1}^{N_{part}}$ are drawn from a *priori* probability density function (PDF). Such particles are propagated using the state evolution model and updated with the observation model in order to give the measurements estimates $T\left(\{\boldsymbol{P}_k^i\}_{i=1}^{N_{part}}\right)$ of the measured data. Then, from the SIS procedure, a likelihood function assigns an importance weight $w_k^i = w_k^i\left(T\left(\boldsymbol{P}_k^i\right)\right)$ for $i = 1, \dots, N_{part}$. The set of the updated states and the weights $\{\boldsymbol{P}_k^i, w_k^i\}_{i=1}^{N_{part}}$ represents the *posteriori* density.

However, the sequential application of this particle filter may result in a degeneracy phenomenon: after a few time iterations, all but a few particles have negligible weight. The degeneracy implies that a large computational effort is devoted to update particles whose contribution to the approximation of the *posteriori* density is practically zero ([13] and [52]) and can be attenuated with the application of more particles, what makes the computational costly considerably increase.

A more applicable strategy to overcome this problem is with a resampling step, that involves a mapping of the random pair $\{\boldsymbol{P}_k^i, w_k^i\}$ into $\{\boldsymbol{P}_k^{i*}, N_{part}^{-1}\}$ with uniform weights [50]. This leads to the elimination of particles with low weights and the replication of particles with high weights ($\boldsymbol{P}_k^{i*}$), what can be performed if the number of effective particles (particles with large weights) falls below a certain threshould, or be applied indiscriminately at each instant t_k, representing the so-called sequential importance resampling (SIR) algorithm.

5.1.2 The SIR Algorithm

The steps of the particle filter SIR in the context of this presented work are described in **Figure 2**. Note that the evolution model, represented by the MFS in this present work, is called in every particle generation procedure, where the direct problem is solved $N_{part} = N$ times. This remark highlights the importance of uses fast and accurate methods on sequential estimation approaches.

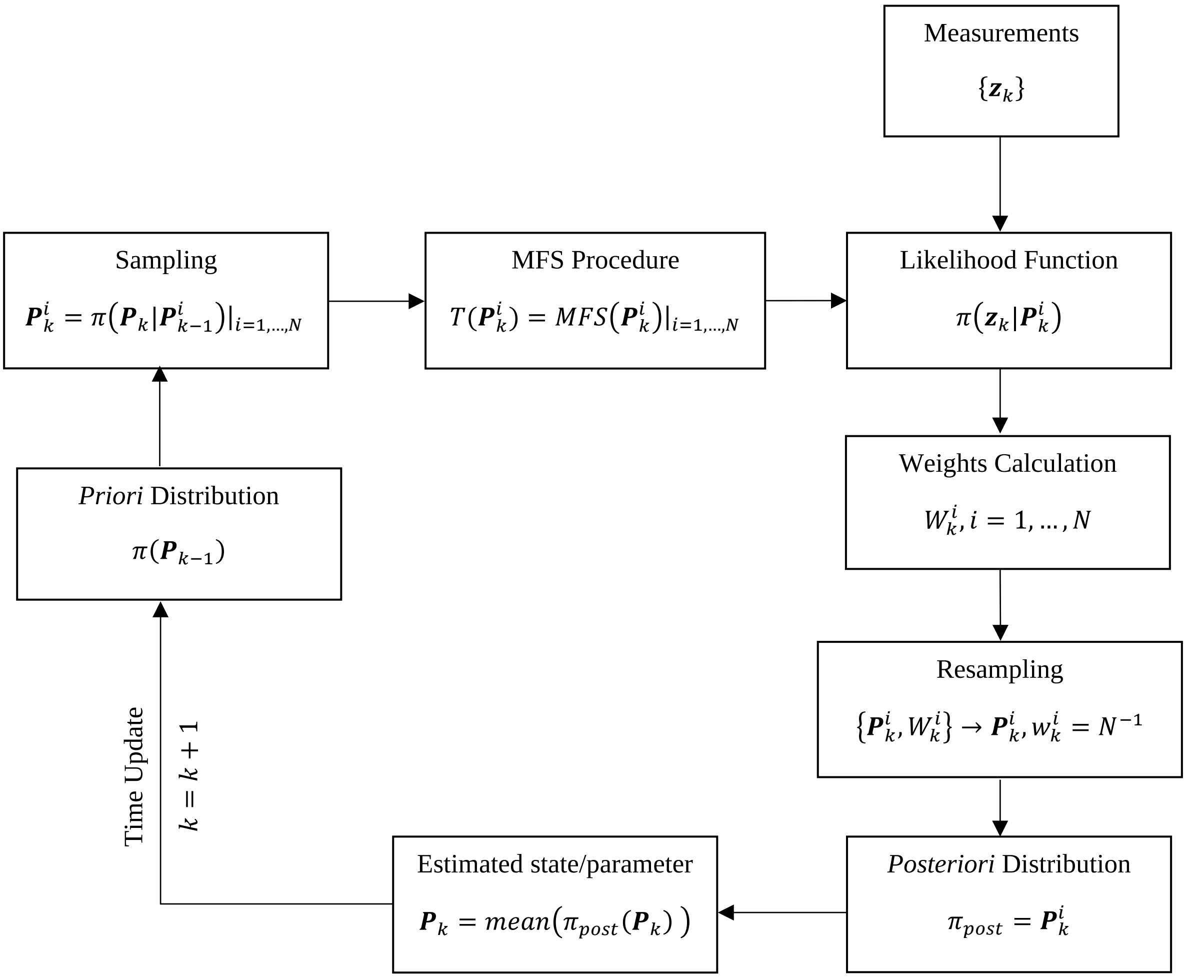

Figure 2 – MFS-PF scheme.

The resampling procedure aims to eliminate the lowest weight particles in order to keep the most important generated particles. A measure from the degeneration of the particles is the effective sample size (N_{eff}), presented in [53], given by

$$N_{eff_k} = \frac{1}{\sum_i^{N_{parti}} \left(w_k^i\right)^2}, \qquad k = 1, \ldots, k_{final}. \tag{5.11}$$

When N_{eff_k} is a low value, it indicates severe degeneration of the particle filter. To evaluate the filter performance, the maximum width of credibility interval ($MWCI$) [54] is determined for each estimated variable, considering the entire period of time.

6 NUMERICAL RESULTS

In this work, first the direct problem is solved in order to obtain information about the MFS implementation and then the inverse problem is solved. In the direct problem, the HTC $\rho(t)$ is known and only the coefficients are unknow and have to be determined by imposing the initial and boundary conditions.

For the direct problem, the root-mean-square error ($RMSE_T$) and the maximum error ($e_{\max}(T)$) of the temperature field is evaluated to the approximation of the sequential MFS to each timestep k, in order to indicate if some instability occurs with the MFS to the respective studied case:

$$RMSE_{\mathrm{T}} = \sqrt{\frac{1}{k_{final}} \sum_{k=1}^{k_{final}} \left(\boldsymbol{T}_k - \widehat{\boldsymbol{T}}_k\right)^2}, \tag{6.1}$$

$$e_{max}(T) = max\left|\boldsymbol{T}_k - \widehat{\boldsymbol{T}}_k\right|_{k=1,\dots,k_{final}}. \tag{6.2}$$

For the inverse problem, the time-dependent HTC ($\rho(t)$) is estimated at same time that the measurements are filtering. The performance related to the efficiency and accuracy of the proposed MFS-PF method is given in terms of root-mean-square error ($RMSE_\rho$) and relative error ($Rel(\rho)$) defined by

$$RMSE_\rho = \sqrt{\frac{1}{k_{final}} \sum_{k=1}^{k_{final}} (\rho - \hat{\rho}_k)^2}, \tag{6.3}$$

$$Rel(\rho) = \frac{\sqrt{\sum_{k=1}^{k_{final}} (\rho_k - \hat{\rho}_k)^2}}{\sqrt{\sum_{k=1}^{k_{final}} \rho_k^2}} \times 100\% \tag{6.4}$$

Thus the N_{eff} is determined (see 5.1.2) along with the maximum width of credibility interval ($MWCI$), to ensure the best performing particle filter:

$$N_{eff_k} = \frac{1}{\sum_i^{N_{parti}} \left(w_k^i\right)^2}, \qquad k = 1, \dots, k_{final}. \tag{6.5}$$

In order to simplify the N_{eff} influence visualization in the results, it will be evaluated in terms of N_{eff}[%], denoting the average percentage relative error between the effective sample size and the total number of particles used.

As an additional diagnostic of the performance of the particle filter, the 95% credibility interval (CI) is presented on the results, and is defined as

$$I_{95\%} = \hat{\rho}_k \pm 1.96\hat{\sigma}_k \;\; k = 1, \dots, k_{final}, \tag{6.6}$$

where $\hat{\rho}_k$ represents the estimated variable and $\hat{\sigma}_k$ represents the uncertainty of the particles. The CI is represented by the shaded region on the estimation/filtering graphical results in this session. For all cases, the number of timesteps for the MFS-PF estimation is $k_{final} = 11$.

6.1 ONE-DIMENSIONAL PROBLEMS

In this section, the simulated measurements are defined by eq.(4.1) or eq.(4.2), where additive or multiplicative types of noisy errors were used:

$$Y_a(t_k) = Y(t_k) + p\varepsilon_k, \qquad k = 1, \dots, k_{final}, \tag{6.7}$$

$$E_a(t_k) = E(t_k) + p\varepsilon_k, \qquad k = 1, \dots, k_{final}, \tag{6.8}$$

$$Y_m(t_k) = Y(t_k)(1 + p\gamma_k), \qquad k = 1, \dots, k_{final}, \tag{6.9}$$

$$E_m(t_k) = E(t_k)(1 + p\gamma_k), \qquad k = 1, \dots, k_{final}, \tag{6.10}$$

where $(\varepsilon_k)_{k=1,\dots,k_{final}}$represents random variables draw from a Gaussian distribution with mean zero and standard deviation

$$\sigma = p \times \begin{cases} max_{k=1,\dots,M}|Y(t_k)|, & \text{in eq. (4.1)}, \quad (a) \\ max_{k=1,\dots,M}|E(t_k)|, & \text{in eq. (4.2)}, \quad (b) \end{cases}, \tag{6.11}$$

p represent the percentage of noise and $\gamma_{k=1,\dots,k_{final}}$ are random variables drawn from a uniform distribution on $[-1,1]$. That way, from the **Table 2**, v_k and n_k are given by a normal distribution of a percentual p of the highest field temperature, considering all time domain.

The representation of one-dimensional problems in the MFS approach is given, for the number of points $M = 12$ and $N = 22$, the final time $t_f = 1$, and the distance from the study domain to the source points given by $d = 0.2$ in **Figure 3**.

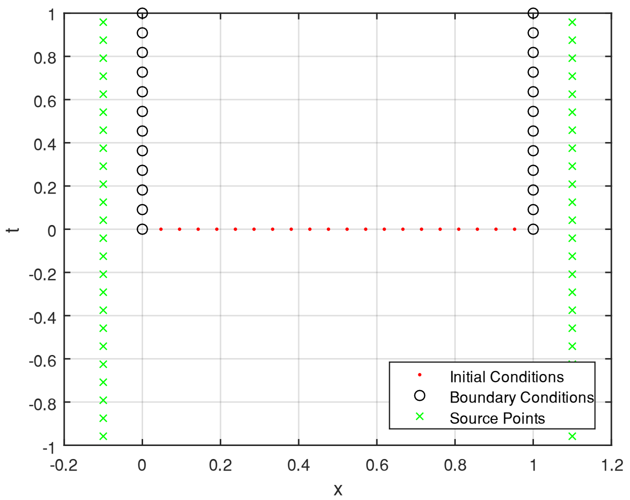

Figure 3 – MFS Scheme with M = 12, N = 22, $t_f = 1$, and $d = 0.2$.

The inverse and direct problems of cases above were performed on a computer with Intel® Core i5 3230M processor.

6.1.1 Linear Boundary Problem

This case is a typical benchmark problem considered in [1], [44], and [55]. Considering the study domain $\Omega \subset [0,1]$, $0 \leq t \leq 1$, and the linear law $g(T) = T$, the initial and boundary conditions are given by

$$\mathrm{T}^0(\mathrm{r}, \theta) = x^2 + 1, \tag{6.12}$$

$$-\frac{\partial T}{\partial x}(0,t) + \rho(t)g\big(T(0,t)\big) = t(2t+1) = h_0(t), \tag{6.13}$$

$$\frac{\partial T}{\partial x}(1,t) + \rho(t)g\big(T(1,t)\big) = 2 + 2t(t+1) = h_1(t), \tag{6.14}$$

and the boundary temperature measurements eq.(4.1) and eq.(4.2):

$$Y(t) = T(1,t) = 2 + 2t, \qquad t \in \big[0, t_f = 1\big), \tag{6.15}$$

$$E(t) = \frac{T^2(0,t) + T^2(1,t)}{2} = \frac{8t^2 + 12t + 5}{2}, \qquad t \in \big[0, t_f = 1\big), \tag{6.16}$$

with the analytical solution given by:

$$T(x,t) = x^2 + 2t + 1, \qquad \rho(t) = t. \tag{6.17}$$

The MFS is applied with $M = 11$, $N = 2M - 2 = 20$ with d varying from 0.2 to 1.4 in order to reach better results for the approximation. The errors from eq.(6.1) and eq.(6.2) are shown in **Table 3**. Note that $e_{max} < 1e - 2$ and $RMSE < 1e - 3$ for $h \geq 1$, therefore assuming $d = 1$, the source points are uniformly located on $y_0 = -1$ and $y_1 = 2$.

Table 3 – d analysis for direct problem 6.1.1 with $M = 11$ and $N = 20$.

$\boldsymbol{d}$	0.2	0.4	0.6	0.8	1	1.2	1.4
$\boldsymbol{RMSE}$	0.022658	0.011539	0.002727	0.001428	0.000310	0.000013	0.000004
$\boldsymbol{e_{max}}$	0.642529	0.335123	0.057974	0.028982	0.009327	0.003021	0.001013

In this problem, the resultant system is solved using SVD with Tikhonov regularization. The λ parameter is selected by the L-curve analysis (**Figure 4**). The parameter chosen is $\lambda = 1e - 12$. The approximation of MFS to direct problem can be verified in **Figure 5** to various coordinates of time and spatial domain.

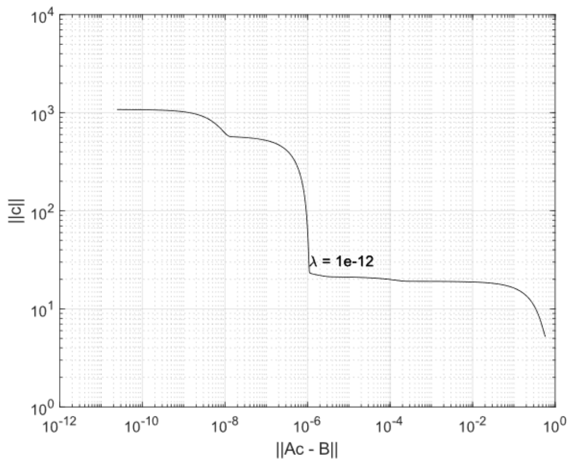

Figure 4 – L-curve for $d = 1$ in 6.1.1.

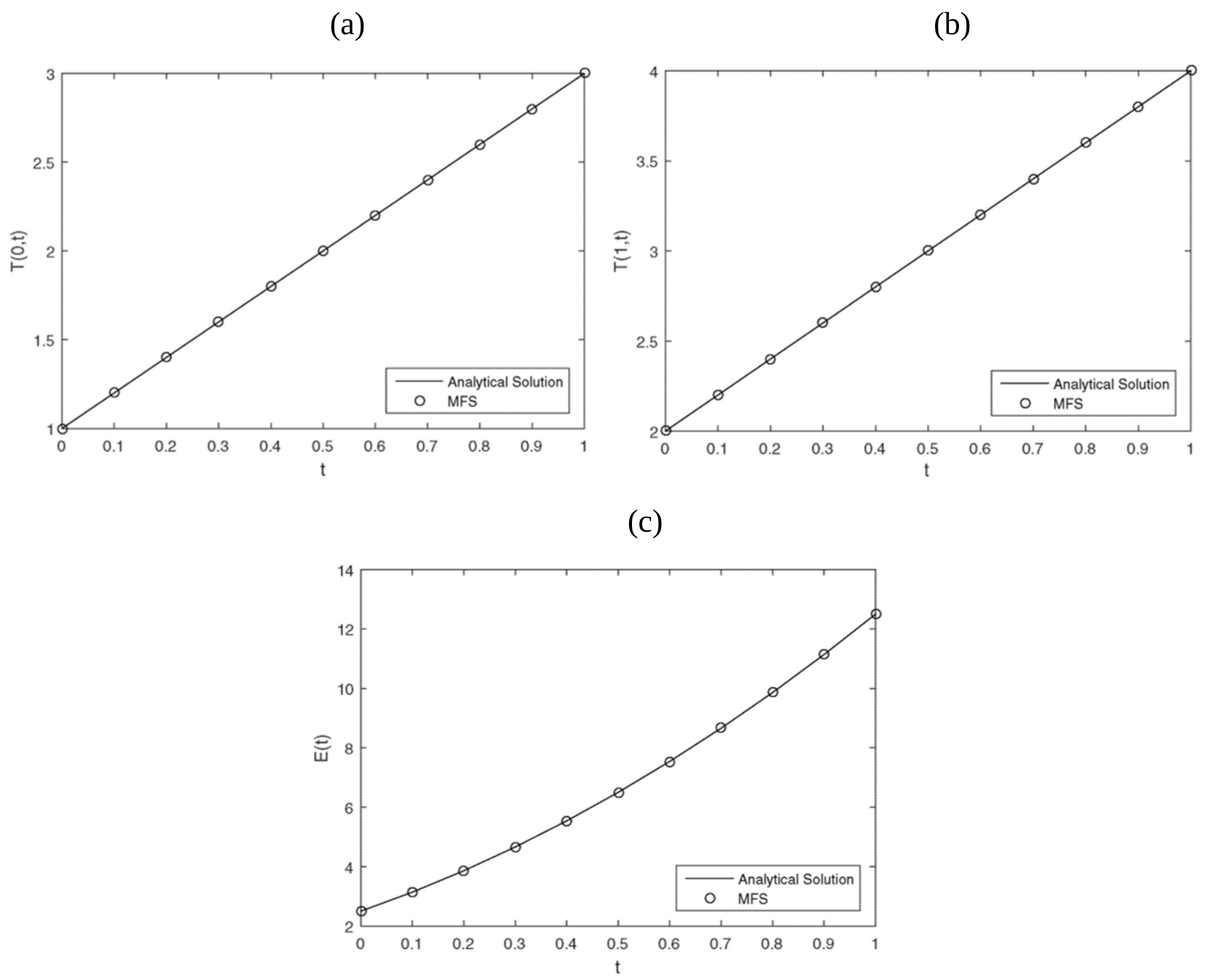

Figure 5 – MFS solution and analytical solution for (a) $T(0,t)$, (b) $T(1,t)$, and (c) $E(t)$, for problem 6.1.1.

Next, we investigate the inverse problem for the standard measurements eq.(6.15). First, an analysis to choose the random walk parameter σ_ρ to the evolution model for $\rho(t)$. We consider the additive noise error measurement eq.(6.7) with $p = 1\%$ noise. We have tested three different standard deviations $\sigma_\rho \in \{0.02, 0.2, 0.4\}$ for the random walk in order to avoid sample impoverishment. When sample impoverishment takes place, most of the particles are eliminated during the resampling step, and a main goal is keep the N_{eff} over 50% of N_{part} [13].

The **Table 4** shows the result of evaluation criteria. Note that $\sigma_\rho = 0.02$ gives inaccurate results, indicating that the random walk does not could be estimated for low values of σ_ρ, because the evolution model for the HTC depends strongly on the *priori* information. This can be verified in the N_{eff}, that is lower than 50% for this case, therefore the search field of the HTC was not fully explored.

Table 4 – SIR results for 6.1.1 with standard measurements: $\sigma \in \{0.02, 0.2, 0.4\}$ for $p = 1\%$.

$\boldsymbol{N_{part}}$	$\boldsymbol{\sigma}$	$\boldsymbol{RMSE_\rho}$	$\boldsymbol{Rel(\rho)}$%	$\boldsymbol{MWCI}$	$\boldsymbol{Neff}$[%]
50	0.02	0.498	70.4	0.14	17.81
100	0.02	0.501	70.9	0.15	17.33
200	0.02	0.490	69.4	0.16	16.26
50	0.2	0.055	7.80	0.30	73.03
100	0.2	0.053	7.40	0.27	74.80
200	0.2	0.052	7.30	0.26	75.20
50	0.4	0.062	8.70	0.47	60.55
100	0.4	0.062	8.78	0.50	60.56
200	0.4	0.053	7.60	0.41	62.27

For illustration, the results obtained by SIR filter with $N_{part} = 200$ and $\sigma = 0.2$ are shown in **Figure 6**, and $\sigma = 0.4$ in **Figure 7**. Once the dynamic behavior of the random walk model improves, the filter is able to draw particles close to the actual HTC with suitable performance. We take $\sigma_\rho = 0.2$.

(a) (b)

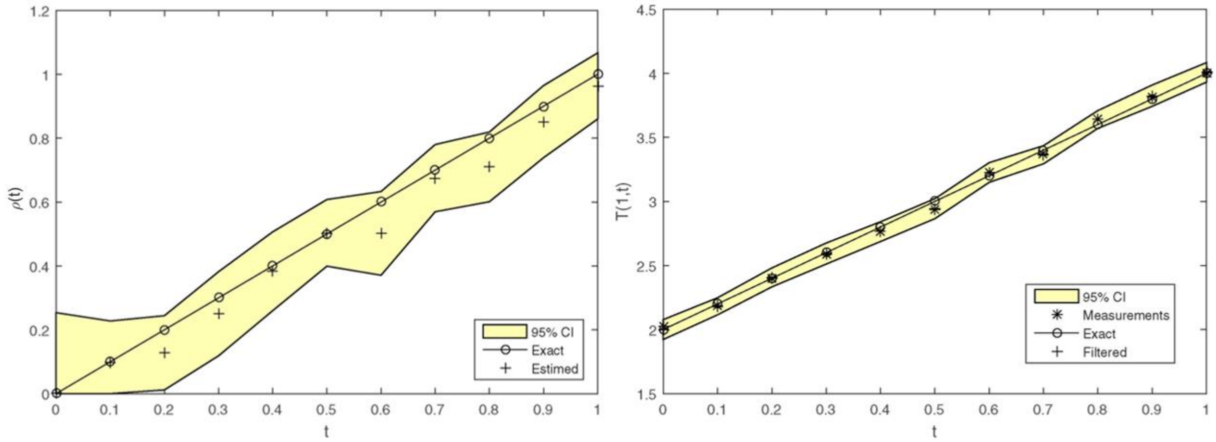

Figure 6 – (a) Estimated $\rho(t)$ and (b) filtered measurements with $p = 1\%$, $\sigma_\rho = 0.2$, and $N_{part} = 200$, for problem 6.1.1.

(a) (b)

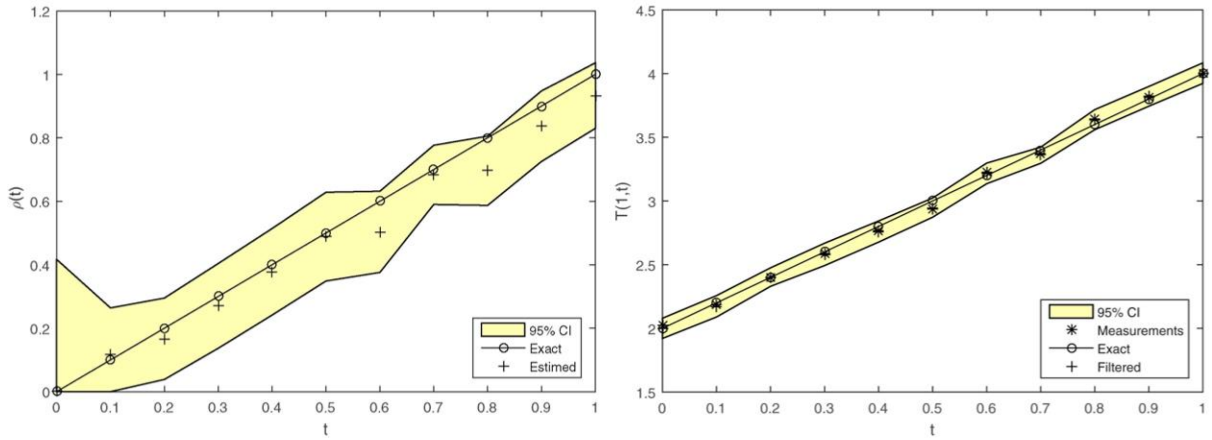

Figure 7 – (a) Estimated $\rho(t)$ and (b) filtered measurements $T(1,t)$ with $p = 1\%$, $\sigma_\rho = 0.4$, and $N_{part} = 200$, for problem 6.1.1.

The SIR results are shown in **Table 5** for $p = 5\%$ and additive noise (eq.(6.7)) and $\sigma_\rho = 0.2$. Note that there was no sample impoverishment, because N_{eff} is always greater than 50%.

Table 5 – SIR results for 6.1.1 with standard measurements $\sigma = 0.2$, for $p = 5\%$

$\boldsymbol{N_{part}}$	$\boldsymbol{p}$	$\boldsymbol{RMSE_\rho}$	$\boldsymbol{Rel(\rho)}$%	$\boldsymbol{MWCI}$	$\boldsymbol{Neff}$[%]
50	5%	0.130	18.40	0.62	74.24
100	5%	0.140	19.80	0.60	72.82
200	5%	0.122	17.30	0.56	75.70

Then, we investigate the non-standard boundary measurements from eq.(6.16). For $\sigma_\rho = 0.2$ contaminated with additive noise from eq.(6.8). The results for $p = \{1, 5\}\%$ are shown in **Table 6**. The SIR results are illustrated for $N_{part} = 200$ and $p = 1\%$ in **Figure 8**.

Table 6 – SIR results for 6.1.1 with non-standard measurements: $\sigma = 0.2$, $p = \{1, 5\}\%$

N_{part}	p	$RMSE_\rho$	$Rel(\rho)\%$	$MWCI$	$Neff[\%]$
50	1%	0.067	9.50	0.28	85.67
100	1%	0.055	7.80	0.27	85.56
200	1%	0.052	7.40	0.24	84.69
50	5%	0.108	15.30	0.54	58.43
100	5%	0.107	15.10	0.51	63.85
200	5%	0.103	14.60	0.51	61.17

(a) (b)

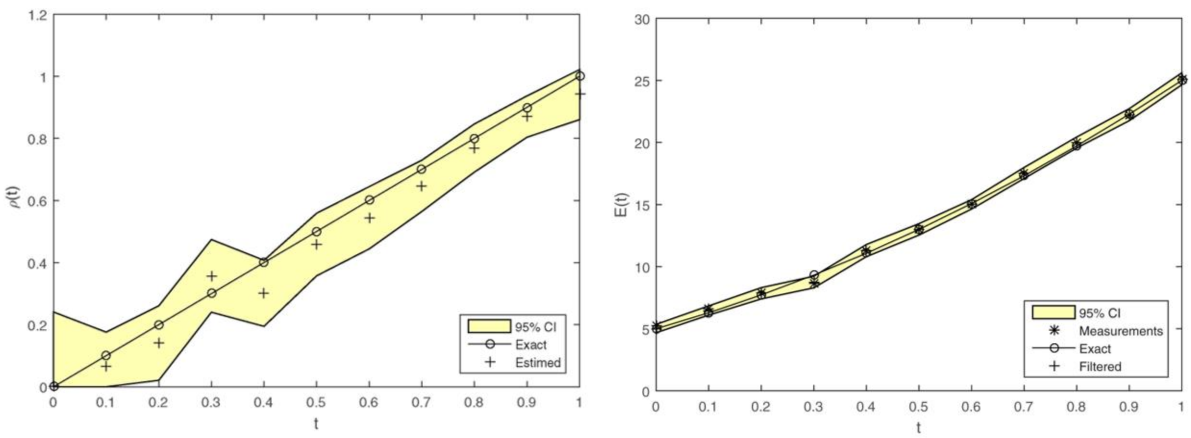

Figure 8 – (a) Estimated $\rho(t)$ and (b) filtered measurements $E(t)$ with $p = 1\%$, $\sigma_\rho = 0.4$, and $N_{part} = 200$, for problem 6.1.1.

The results obtained from the multiplicative noise from eq.(6.11) – (a) for the standard measurements and (b) for non-standard – contaminating with $p = 5\%$ are shown in **Table 7**.

Table 7 – SIR results for 6.1.1 with multiplicative errors: $\sigma = 0.2$, $p = 5\%$.

$\boldsymbol{N_{part}}$	Equation	$\boldsymbol{RMSE_{\rho}}$	$\boldsymbol{Rel(\rho)}$%	$\boldsymbol{MWCI}$	$\boldsymbol{Neff}$[%]
50	(a)	0.103	14.60	0.54	74.98
100	(a)	0.096	13.60	0.54	76.34
200	(a)	0.079	11.10	0.54	75.39
50	(b)	0.044	6.20	0.41	53.26
100	(b)	0.038	5.30	0.38	54.93
200	(b)	0.037	5.30	0.34	52.96

The graphics for $N_{part} = 200$ in the case (a) and case (b) are shown in **Figure 9** and **Figure 10**, respectively. Note that the non-standard measurements represents a highest accuracy related to the standard measurements, and the CI is lower and closest to the aimed value, what can be viewed in the lower $MWCI$ from case (b).

The N_{eff} value from case (b) is lower than in case (a), but higher than 50%, indicating that the degeneracy phenomenon do not spoil the results from the estimation.

(a) (b)

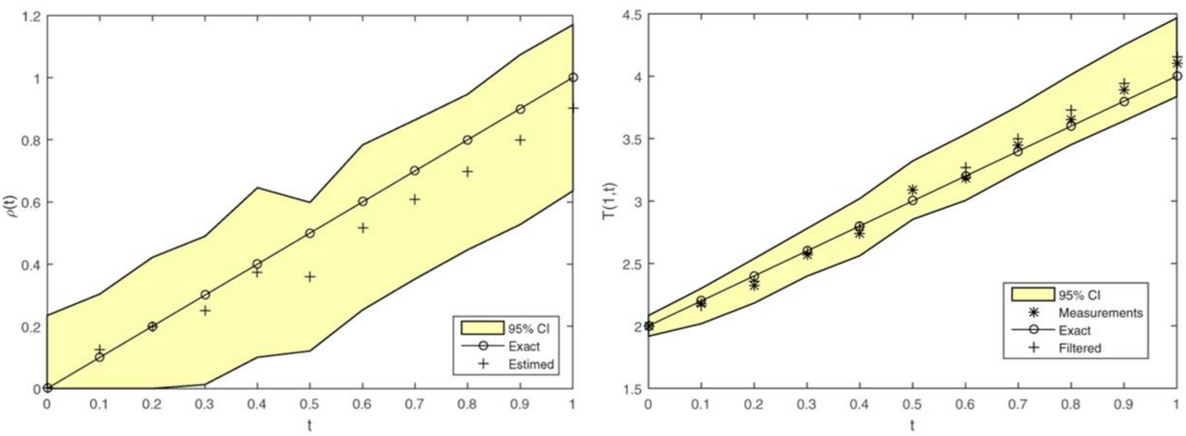

Figure 9 – (a) Estimated $\rho(t)$ and (b) filtered measurements $T(1,t)$ with multiplicative noise $p = 5\%$, $\sigma_{\rho} = 0.2$, and $N_{part} = 200$, for problem 6.1.1.

(a) (b)

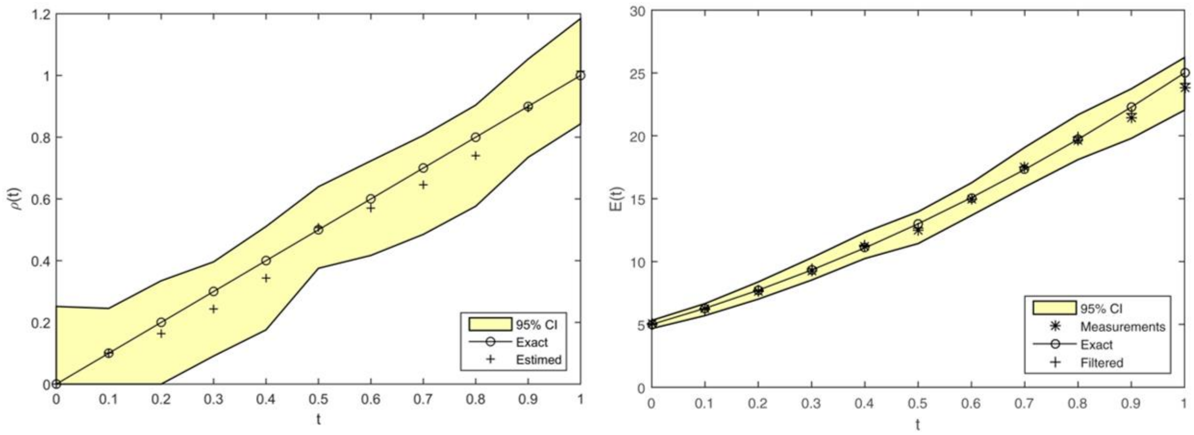

Figure 10 – (a) Estimated $\rho(t)$ and (b) filtered measurements $E(t)$ with multiplicative noise $p = 5\%$, $\sigma_\rho = 0.2$, and $N_{part} = 200$, for problem 6.1.1.

The graphics for $N_{part} = 200$ in the case (a) and case (b) with $p = 5\%$ with $\sigma_\rho = 0.4$ are plotted to compare with the $\sigma_\rho = 0.2$ results. They are shown in **Figure 11** and **Figure 12**, respectively. This present results shown same behavior of previously see in **Table 4**, where $\sigma_\rho = 0.2$ presented better results than $\sigma_\rho = 0.4$, with lower $MWCI$ values.

(a) (b)

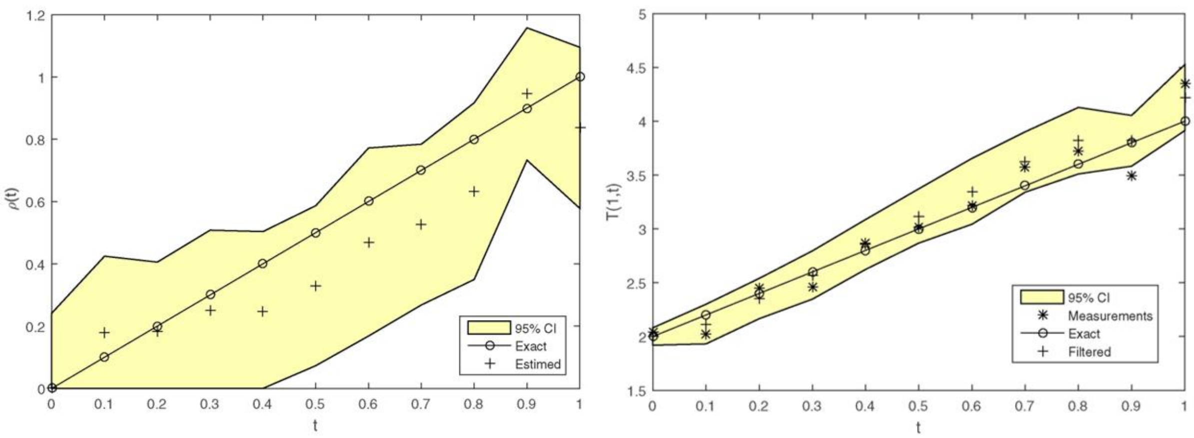

Figure 11 – (a) Estimated $\rho(t)$ and (b) filtered measurements $T(1,t)$ with $p = 5\%$, $\sigma_\rho = 0.4$, and $N_{part} = 200$, for problem 6.1.1.

(a) (b)

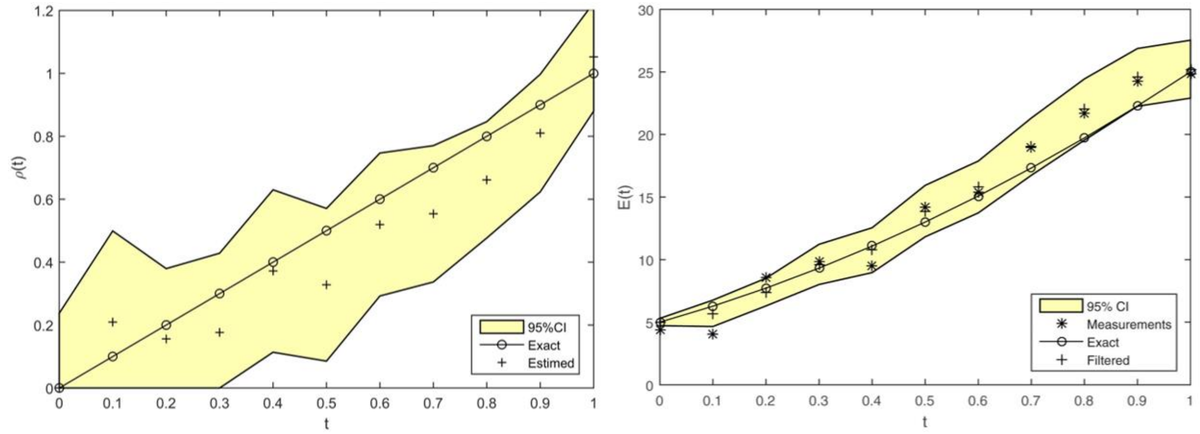

Figure 12 – (a) Estimated $\rho(t)$ and (b) filtered measurements $E(t)$ with $p = 5\%$, $\sigma_\rho = 0.4$, and $N_{part} = 200$, for problem 6.1.1.

In general way, the HTC could be estimated in all cases, including using multiplicative noise. The use of the non-standard measurements makes the $MWCI$ decreases in relation to the standard measurements, indicating that the non-standard measurement contains more information in the inverse problem than the standard measurement.

The computational cost for 200 particles were on average 547 seconds, indicating that the time to propagate each particle through MFS to the problem was inferior than 0.28 seconds.

It's possible to compare the obtained results with the same problem studied by Yan *et al.* [55], that uses Bayesian MCMC inference approach in a similar case. In the previous work, the relative error $Rel(\rho) \in \{3.84, 8.07\}\%$ for $p \in \{1, 5\}\%$, lower than the better results obtained by MFS-PF, that are $Rel(\rho) \in \{7.81, 17.30\}\%$ for $p \in \{1, 5\}\%$. Although the worst results, the MFS-PF represents a lower computational cost compared to MCMC, that uses all the time history measurements globally, being a reliable method for offline problems, and it has also resulted in some negative values for the estimated HTC, which are physically unrealistic.

In Onyango *et al.* [1], where the HTC is estimated in a BEM framework, same negative HTC problem happened when no positivity constant or regularization is imposed. In the MFS-PF algorithm neither negativity nor instability happened.

6.1.2 Nonlinear Boundary Problem

In the nonlinear case, we aim to solve a problem previously presented in [2].

Considering the study domain $\Omega \subset [0,1]$, $0 \leq t \leq 1$, and the nonlinear radiation $g(T) = T^3|T|$, the initial and boundary conditions are given by

$$T^0(x) = x^2, \qquad x \in [0,1], \tag{6.18}$$

$$-\frac{\partial T}{\partial x}(0,t) + \rho(t)g\big(T(0,t)\big) = 16t^4(t+1) = h_0(t), \tag{6.19}$$

$$\frac{\partial T}{\partial x}(1,t) + \rho(t)g\big(T(1,t)\big) = (1+t)(1+2t)^4 + 2 = h_1(t) \tag{6.20}$$

and the boundary temperature measurements from eq.(4.2)

$$E(t) = 12.8t^5 + 16t^4 + 8t^2 + 2t + 0.2 \tag{6.21}$$

with the analytical solution given by

$$T(x,t) = x^2 + 2t, \qquad \rho(t) = 1 + t, \tag{6.22}$$

For this nonlinear MFS direct problem, we impose $M = 12$, $N = M - 2 = 10$ with d varying from 0.2 to 1.4 in order to reach better results for the approximation. The errors from eq.(6.1) and eq.(6.2) are shown in **Table 8**. Note that $e_{max} < 1e-2$ and $RMSE < 1e-4$ for $h \geq 1$, therefore assuming $d = 1$, the source points are uniformly located on $y_0 = -1$ and $y_1 = 2$. In this problem, the resultant system is solved using $fmincon$ toolbox from MATLAB using the Levenberg-Marquardt method. The accuracy of the direct problem using MFS can be verified in **Figure 13** to the temperature in $x = 0$, $x = 1$ and the non-standard measurement calculation.

Table 8 – d analysis for direct problem 6.1.2 with $M = 12$ and $N = 10$.

d	0.2	0.4	0.6	0.8	1	1.2	1.4
$\boldsymbol{RMSE}$	0.00332	0.00260	0.00114	0.00070	0.00009	0.00005	0.00001
$\boldsymbol{e_{max}}$	0.13277	0.06906	0.02738	0.03114	0.00707	0.00316	0.00315

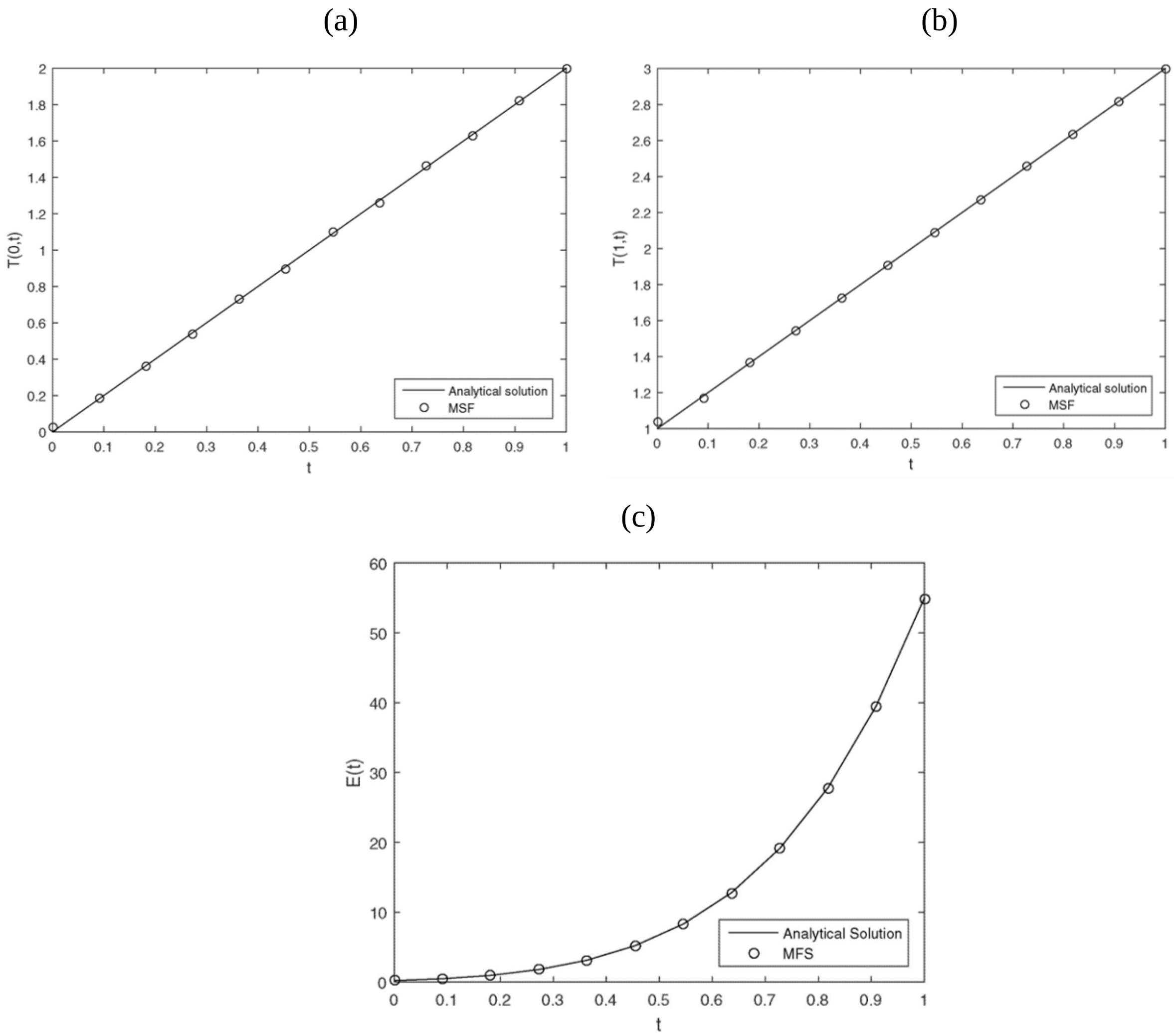

Figure 13 – MFS solution and analytical solution for (a) $T(0,t)$, (b) $T(1,t)$, (c) $E(t)$, for problem 6.1.2.

The inverse problem is solved using $p \in \{5, 10\}\%$, and the results are shown in **Table 9** using the better resulting $\sigma_\rho = 0.2$ from session 6.1.1, where the HTC have the same behavior.

Table 9 – SIR results 6.1.2 for multiplicative error from eq.(6.10): $\sigma = 0.2$, $\rho \in \{5,10\}\%$.

N_{part}	p	$RMSE_\rho$	$Rel(\rho)\%$	$MWCI$	$Neff[\%]$
50	5%	0.041	16.40	0.94	74.28
100	5%	0.030	13.90	0.82	72.83
200	5%	0.027	13.40	0.77	75.70
50	10%	0.061	20.00	0.87	53.06
100	10%	0.055	18.90	0.84	54.80
200	10%	0.054	18.80	0.81	55.20

The graphics for $N_{part} = 200$ with $p = 5\%$ and $p = 10\%$ are represented in **Figure 14** and **Figure 15**, respectively. This p values represent the same values from the reference [2].

(a) (b)

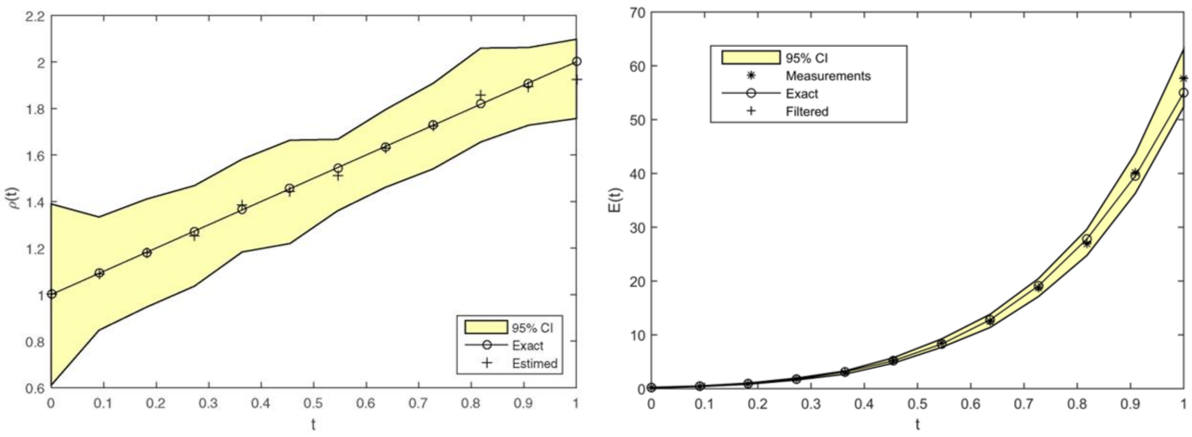

Figure 14 – (a) Estimated $\rho(t)$ and (b) filtered measurements $E(t)$ with multiplicative noise $p = 5\%$, $\sigma_\rho = 0.2$, and $N_{part} = 200$, for problem 6.1.2.

(a) (b)

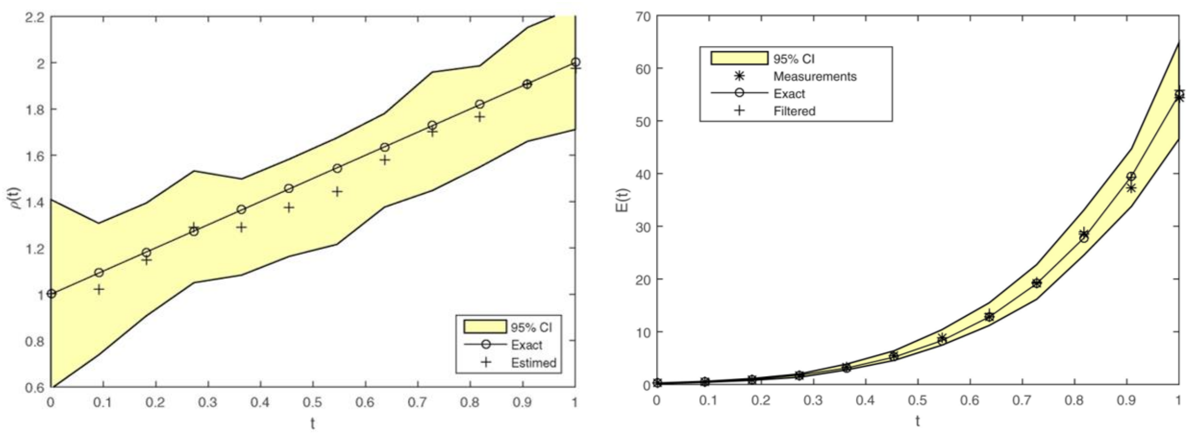

Figure 15 – (a) Estimated $\rho(t)$ and (b) filtered measurements $E(t)$ with multiplicative noise $p = 10\%$, $\sigma_\rho = 0.2$, and $N_{part} = 200$, for problem 6.1.2.

The computational cost for 200 particles were on average 844 seconds, indicating that the time to propagate each particle through MFS to the problem was inferior than 0.43 seconds, representing an increase of 54% in comparison of linear case in 6.1.1.

The results shown good stability and are comparable in terms of accuracy with the results obtaining by a nonlinear BEM with a posterior Tikhonov regularization from [2], shown in **Figure 16**. In this figure, the $\sigma(t)$ axis correspond to the HTC ($\rho(t)$ in this present work), and the multiplicative noise is correspondent to ρ.

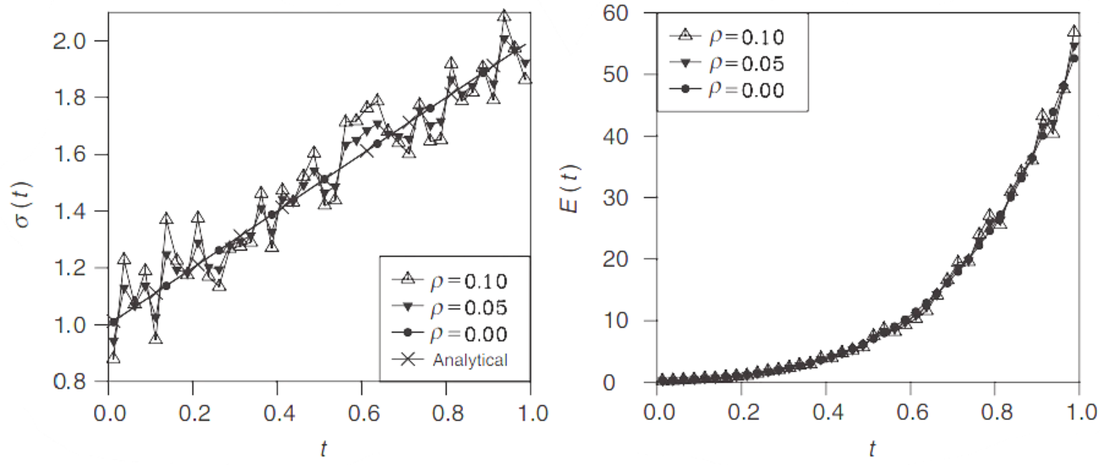

Figure 16 – Estimation by Slodicka et al. [2].

6.2 MULTIDIMENSIONAL PROBLEMS

In multidimensional problems, the simulated measurements are defined only by the non-standard measurement eq.(4.6), and additive noisy errors were used:

$$E_a(t_k) = E(t_k) + \varepsilon_k, \qquad k = 1, \dots, k_{final}, \tag{6.23}$$

where $(\varepsilon_k)_{k=1,\dots,M}$represents random variables drawn from a Gaussian distribution with mean zero and standard deviation is given by

$$\sigma = p \times max_{k=1,\dots,k_{final}} |E(t_k)|. \tag{6.24}$$

where p represent the percentage of noise. That way, from the **Table 2**, v_k and n_k are given by a normal distribution of a percentual p of the highest field temperature, considering all time domain.

In this session, the standard deviation σ_ρ is not given as a constant, but is drawn from a uniform distribution between 0.05 and 0.2. This hypothesis was adopted assuming that we know a *priori* that the maximum value of the HTC is equal to unity. Such that the lower limit corresponds to 5% of this. On the other hand, if the HTC suddenly changes over time, the parameter search field should be broadened, so that 20% of the maximum allowable value is used as an upper limit.

The representation of one-dimensional problems in the MFS approach is given, for the number of points $M = 12$, $N = 22$ and the distance from the study domain to the source points given by $d = 0.2$ in **Figure 17**.

The inverse and direct problems of cases above were performed on a computer with Intel® Core i5 8265U processor.

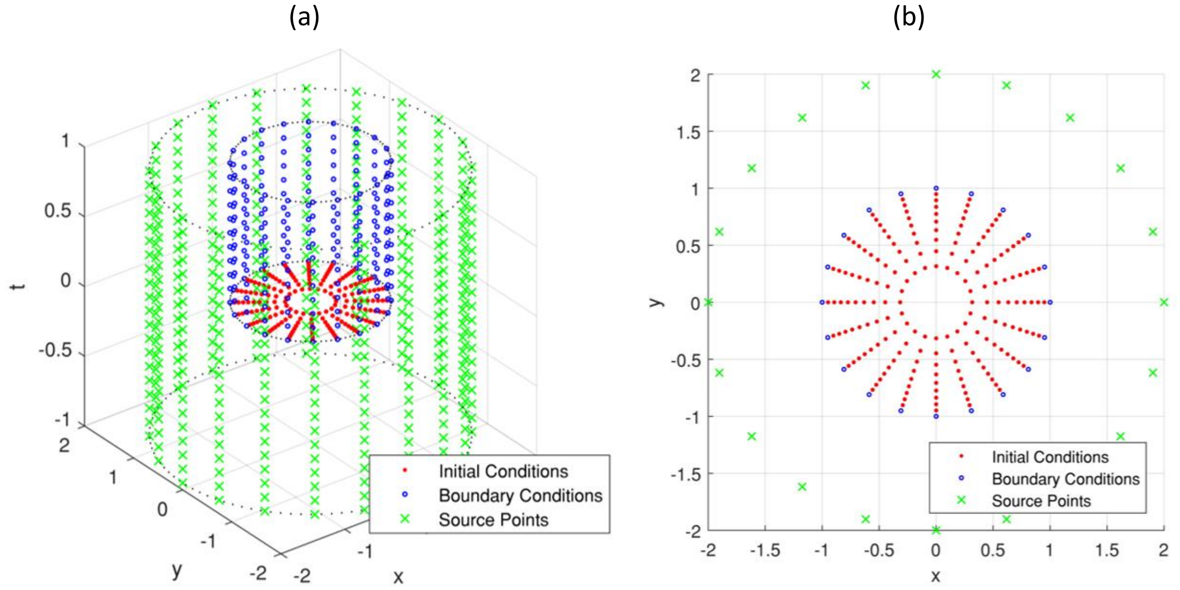

Figure 17 – Multidimensional scheme with M = 10, N = 10, $t_f = 1$, $r_0 = 1$, and $h = 1$, centered in $(0,0,t)$. (a) (x, y, t) view, and (b) (x, y) view.

6.2.1 Linear Boundary Problem

Considering a circular domain, where $0 \leq r \leq 1$, and $0 \leq t \leq 1$. The system corresponds to the linear law $g(T) = T$, and the initial and boundary condition are given by

$$T^0(r, \theta) = r^2 + 1, \tag{6.25}$$

$$h(r, \theta, t) = 2 + t(2 + 4t). \tag{6.26}$$

The non-standard measurement is given by

$$E(t) = \pi(2+4t)^2, \;\; t \in \left[0, t_f = 1\right), \tag{6.27}$$

and the analytical solution of the inverse problem is given by

$$T(r,\theta,t) = r^2 + 4t + 1, \qquad \rho(t) = t. \tag{6.28}$$

The direct problem considers that the information in eq.(6.28) for the HTC**Error! Reference source not found.** is well known. The MFS is applied with $M = 10$, $N = 20$ with d varying from 5 to 11 in order to reach better results for the approximation. The resulting system of MFS is solved using SVD with Tikhonov regularization. The errors from eq.(6.1) and eq.(6.2) are shown in **Table 10**. Note that as from $d = 10$, the e_{max} and $RMSE$ starts to increase. Assuming $d = 10$, we can set the regularization parameter λ from L-curve analysis (**Figure 18**). The parameter chosen is $\lambda = 1e - 12$.

Table 10 – d analysis for direct problem 6.2.1 with $M = 10$ and $N = 20$.

d	5	6	7	8	9	10	11
$\boldsymbol{RMSE}$	0.0182	0.0041	0.0030	0.0023	0.0016	0.0021	0.0036
$\boldsymbol{e_{max}}$	0.0974	0.0282	0.0173	0.0127	0.0098	0.0095	0.0632

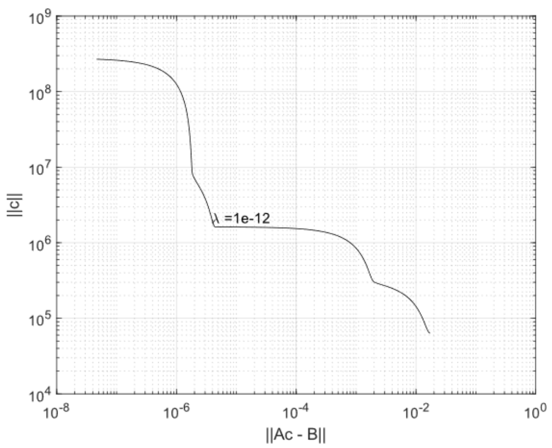

Figure 18 – L-curve for $d = 10$ in 6.2.1.

The MFS accuracy for the direct problem can be verified on **Figure 19**, that compares the analytical solution for the non-standard measurement eq.(6.27) with the respective MFS numerical solution obtained from $d = 10$ and $\lambda = 1e - 12$. Same parameters are used to show the temperature field in the last timestep, that is compared with the analytic response in the **Figure 20**.

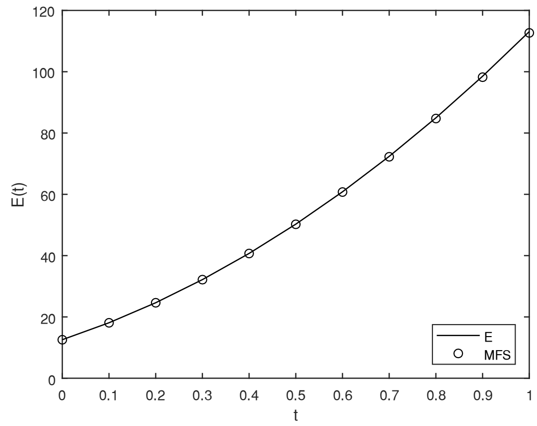

Figure 19 – Direct problem 6.2.2, $E(t)$ analytical and numerical for $h = 10$, $\lambda = 1e - 12$.

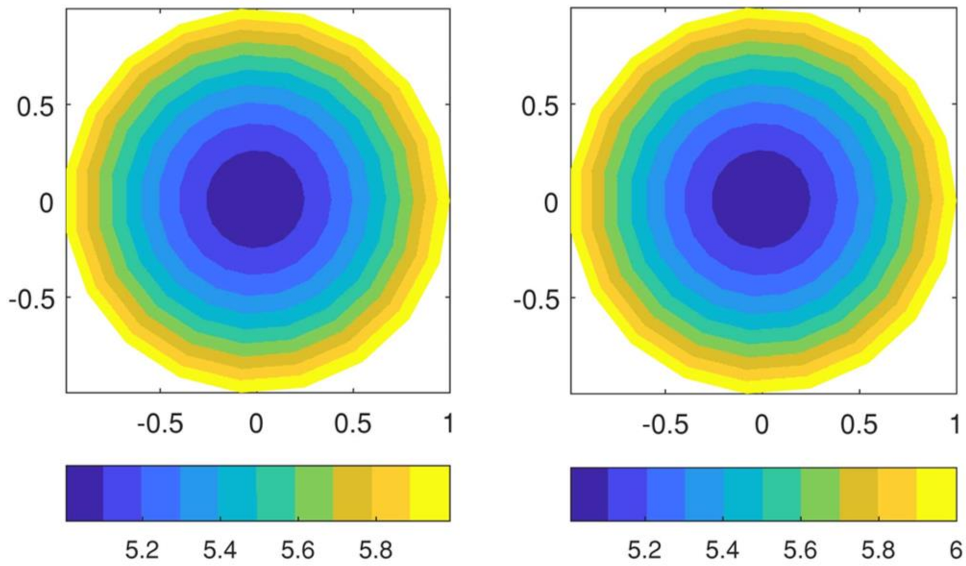

Figure 20 –Sequential MFS for Direct problem (left) and the analytical response (right) of **6.2.1**, with $t = t_{final}$.

Next, we investigate the inverse problem. Imposing $N_{part} = \{50, 100, 200, 400\}$, and using the random walk as uniform distribution function, the results from **Table 11** are given for $p = \{1, 5\}\%$.

Table 11 – SIR results for 6.2.1 with $p \in \{1\%, 5\%\}$.

N_{part}	$\boldsymbol{p}$	$RMSE_\rho$	$\boldsymbol{Rel(\rho)}\%$	$MWCI$	$\boldsymbol{Neff}[\%]$
50	1%	0.021	3.56	0.33	54.30
100	1%	0.015	2.66	0.32	50.00
200	1%	0.012	2.03	0.32	63.86
400	1%	0.009	1.56	0.34	58.87
50	5%	0.020	4.72	0.28	51.87
100	5%	0.027	3.54	0.30	50.16
200	5%	0.010	2.53	0.31	50.37
400	5%	0.015	1.70	0.32	51.41

Note that all results had the $N_{eff} > 50\%$ what indicates that there was no sample impoverishment, and the errors decrease substantially when the number of particles increases for $\boldsymbol{p} = 1\%$. For $\boldsymbol{p} = 5\%$ this behavior was not observed for the $RMSE$, having the MFS-PF better results using 200 particles. This result highlights that, as a stochastic method, the particle filter not necessarily have better global results using more particles, but is expected that the results get closer to the real value, what can be observed in the relative error, that decreases when the number of particles increases. The graphic representation of the behavior of σ_ρ for $N_{part} = NP = \{50, 100, 200, 400\}$, and $p = 1\%$ is shown in **Figure 21**.

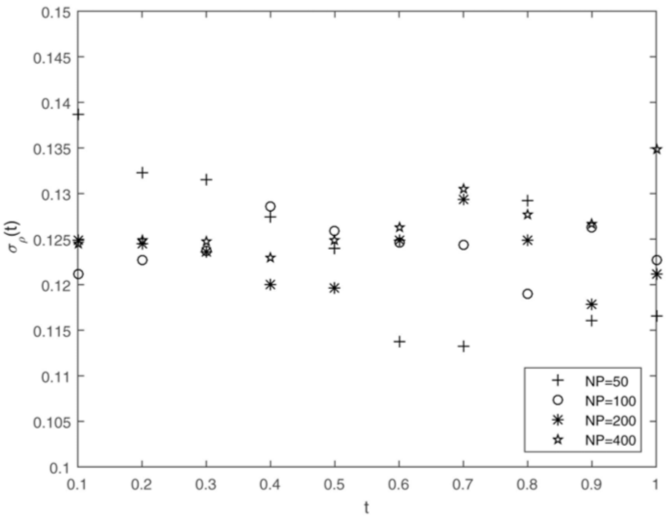

Figure 21 – Behavior of $\sigma_\rho(t)$ over time, with $p = 1\%$.

It's possible to note that the $\sigma_\rho(t)$ converges to $\sigma_\rho \cong 0.125$. The estimation of the HTC and filtering measurements using $N_{part} = 400$ are shown in **Figure 22** for $p = 1\%$.

(a) (b)

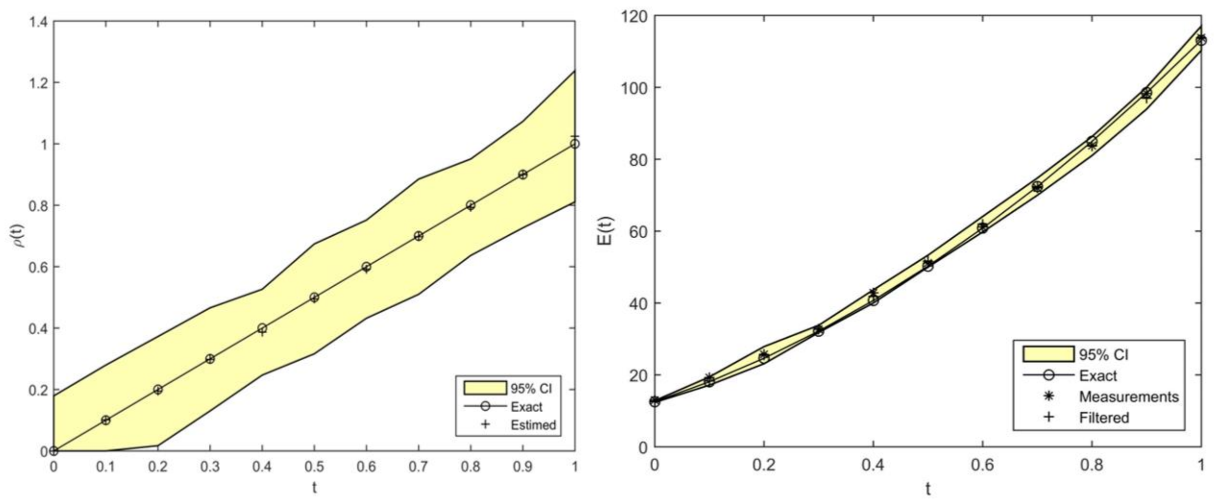

Figure 22 – (a) Estimated $\rho(t)$ and (b) filtered measurements $E(t)$ with $p = 1\%$ and $N_{part} = 400$, for problem 6.2.1.

The behavior of σ_ρ for $p = 5\%$ and the graphical representation of this case with $N_{part} = 400$ are shown in **Figure 23** and **Figure 24**, respectively.

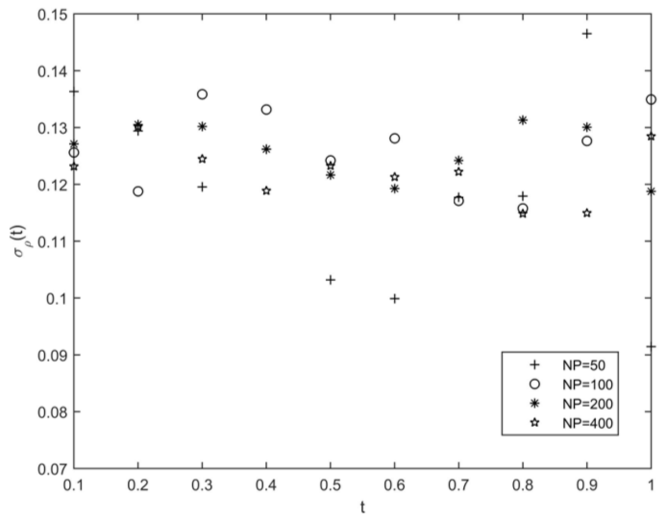

Figure 23 – Behavior of $\sigma_\rho(t)$ over time, with $p = 5\%$.

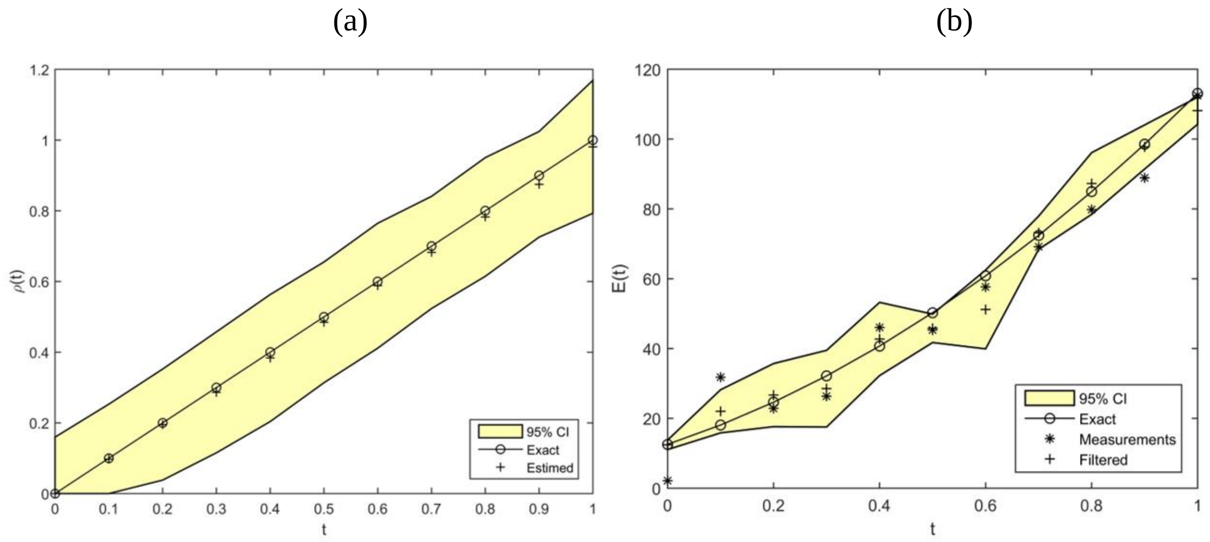

Figure 24 – (a) Estimated $\rho(t)$ and (b) filtered measurements $E(t)$ with $p = 5\%$ and $N_{part} = 400$, for problem 6.2.1.

Even though there was a greater spread of the σ_ρ using greater noise levels, it's possible see that the standard deviation converges to $\sigma_\rho \cong 0.125$. This observation, added to the good filtering and estimated results, clearly shows that the MFS-PF approach provides stable numerical solutions to the inverse Robin problems with convective boundary.

The computational cost for 400 particles were on average 980 seconds, indicating that the time to propagate each particle through MFS to the problem was inferior than 0.25 seconds.

6.2.2 Nonlinear Boundary Problem

Considering a circular domain, where $0 \leq r \leq 1$, and $0 \leq t \leq 1$. The system corresponds to the nonlinear law $g(T) = T^3|T|$, corresponding to radiation, and the initial and boundary condition are given by

$$T^0(\mathrm{r}, \theta) = \mathrm{r}^2, \tag{6.29}$$

$$h(r, \theta, t) = 2 + t(1 + 4t)^4. \tag{6.30}$$

The non-standard measurement is given by:

$$E(t) = \frac{2\pi(1 + 4t)^5}{5}, \tag{6.31}$$

and the analytical solution is given by

$$T(r, \theta, t) = r^2 + 4t, \qquad \rho(t) = t + 1. \tag{6.32}$$

The number of points used is $M = 10$ and $N = 10$. In the direct problem, the resulting system was solved using the MATLAB toolbox *lsqnonlin* with the trust-region-reflective method to deal with the nonlinearity of boundary conditions. The errors from eq.(6.1) and eq.(6.2) varying d from 0.2 to 1.2 are presented in **Table 12**. In this case, the errors presented similar results for all tested d. The distance $d = 1$ is chosen because have the lower $RMSE$.

Table 12 – d analysis for direct problem 6.2.2 with $M = 10$ and $N = 10$.

d	0.2	0.4	0.6	0.8	1	1.2
$\boldsymbol{RMSE}$	0.0331	0.0363	0.0310	0.0315	0.0314	0.0329
$\boldsymbol{e_{max}}$	0.1539	0.1449	0.1292	0.1200	0.1140	0.1063

The MFS accuracy for the direct problem can be visually verified on **Figure 25**, that compares the analytical solution for the non-standard measurement eq.(6.31) with the respective MFS numerical solution obtained from $d = 1$, $M = 10$ and $N = 10$. Same parameters are used to show the temperature field in the last timestep, that is compared with the analytic response in the **Figure 26**.

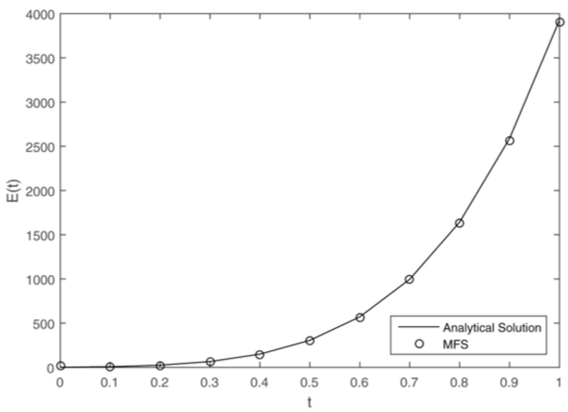

Figure 25 – Direct problem 6.2.2, $E(t)$ analytical and numerical for $h = 1$

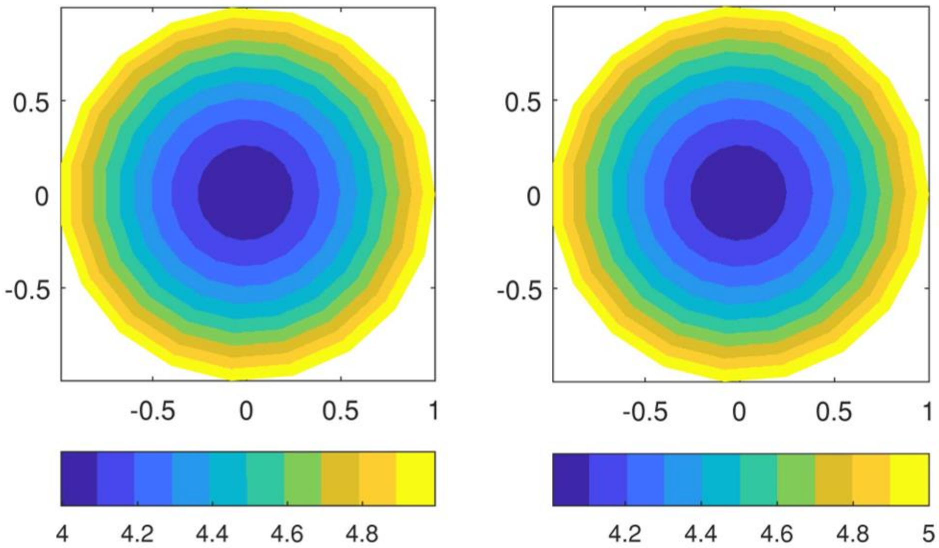

Figure 26 – Sequential MFS for Direct problem (left) and the analytical response (right) of **6.2.2**, with $t = t_{final}$.

Then, imposing $N_{part} = \{50, 100, 200, 400\}$, and using the random walk as uniform distribution function, the results from **Table 13** are given for $p = \{1, 5\}\%$.

Table 13 – SIR results for 6.2.2 with $p \in \{1\%, 5\%\}$.

$\boldsymbol{N_{part}}$	$\boldsymbol{p}$	$\boldsymbol{RMSE_\rho}$	$\boldsymbol{Rel(\rho)}\%$	$\boldsymbol{MWCI}$	$\boldsymbol{Neff}[\%]$
50	1%	0.080	5.24	0.38	93.88
100	1%	0.080	5.22	0.39	92.37
200	1%	0.066	4.35	0.39	92.98
400	1%	0.066	4.32	0.41	93.31
50	5%	0.093	6.09	0.39	95.17
100	5%	0.083	5.45	0.37	94.51
200	5%	0.065	4.26	0.40	94.66
400	5%	0.059	3.58	0.40	94.55

Note that for both error values p, the $RMSE$ and Rel decreases when the number of particles increases. All cases produced $N_{eff} > 50\%$, and similar $MWCI$ values. The graphic representation of the behavior of σ_ρ for $N_{part} = NP = \{50, 100, 200, 400\}$ is shown in **Figure 27**.

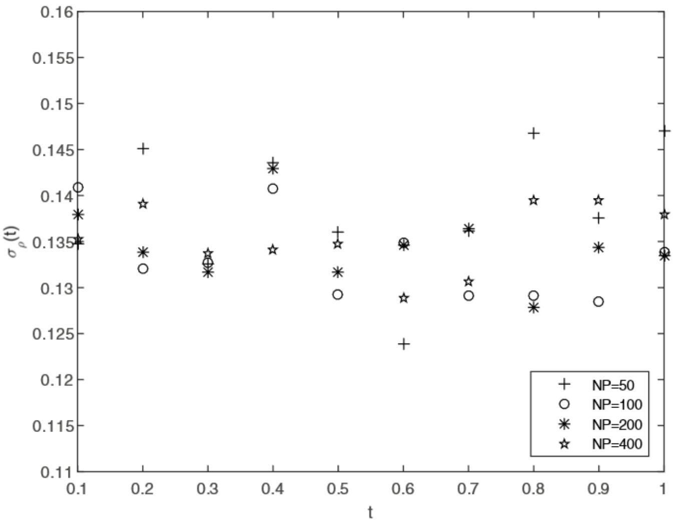

Figure 27 – Behavior of $\sigma_\rho(t)$ over time, with $p = 1\%$ for problem 6.2.2.

It's possible to note that the $\sigma_\rho(t)$ converges to $\sigma_\rho \cong 0.135$. The estimation of the HTC and filtering measurements using $N_{part} = 400$ are shown in **Figure 28** for $p = 1\%$. A detailed view of the filtered results are shown in **Figure 29**.

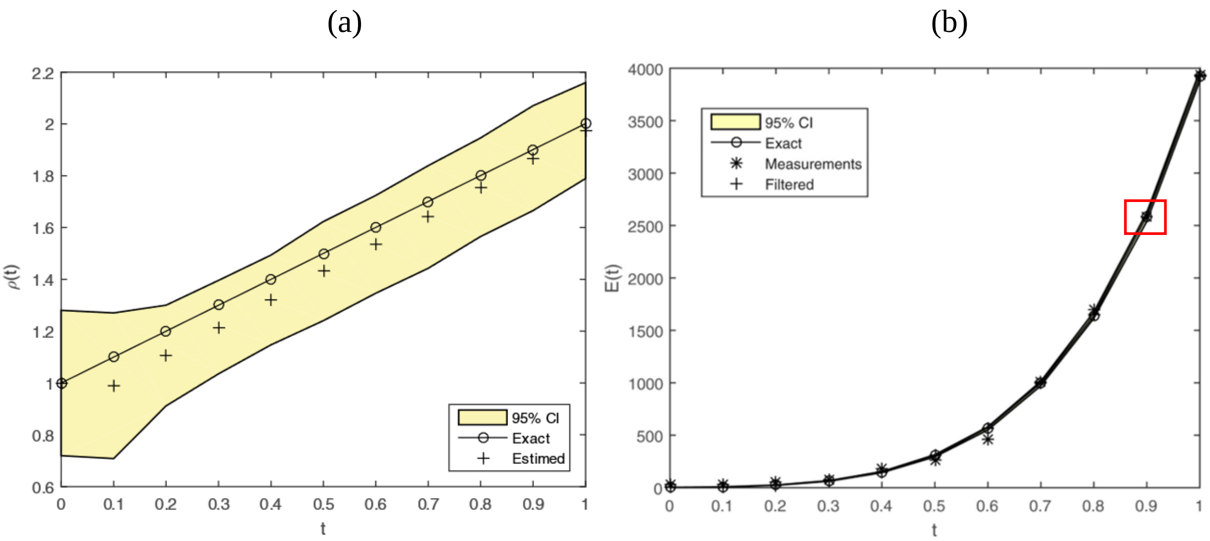

Figure 28 – (a) Estimated $\rho(t)$ and (b) filtered measurements $E(t)$ with $p = 1\%$ and $N_{part} = 400$, for problem 6.2.2.

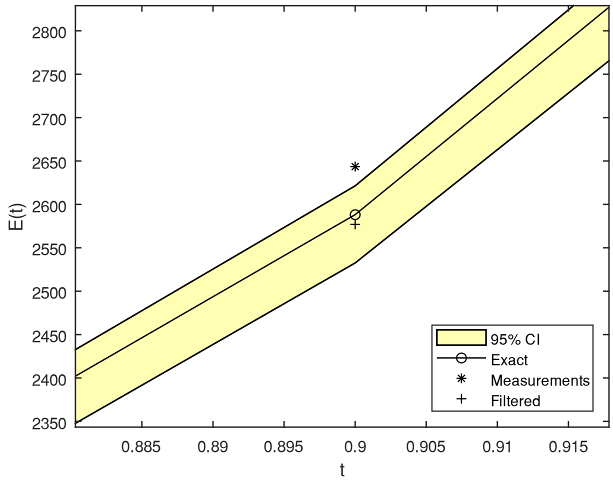

Figure 29 – Detail from the figure **Figure 28** (b).

It is possible to view that the estimation of the HTC have a detachment from the real values especially on the initial timesteps, what is attenuated at highest timesteps. The behavior of σ_ρ for $p = 5\%$ and the graphical representation of this case with $N_{part} = 400$ are shown in **Figure 30** and **Figure 31**, respectively.

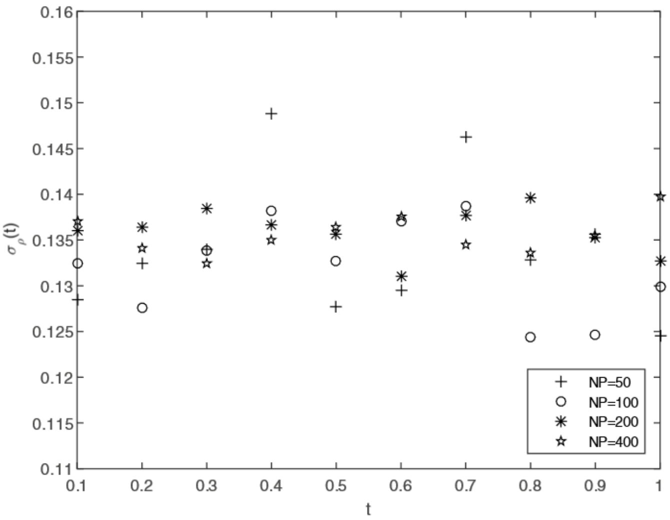

Figure 30 – Behavior of $\sigma_\rho(t)$ over time, with $p = 5\%$ for problem 6.2.2.

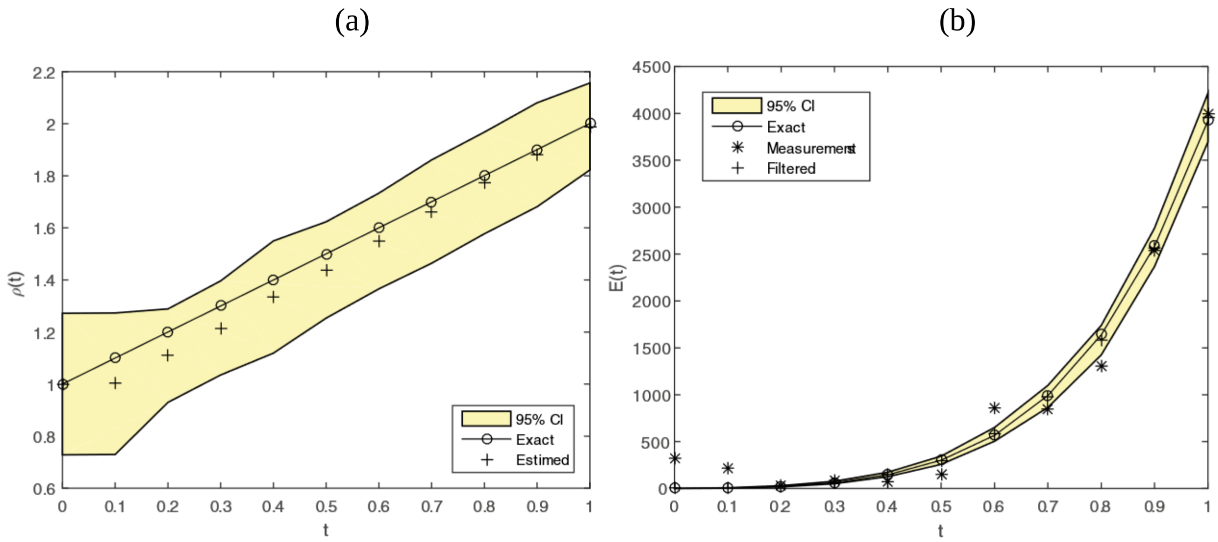

Figure 31 – (a) Estimated $\rho(t)$ and (b) filtered measurements $E(t)$ with $p = 5\%$ and $N_{part} = 400$, for problem 6.2.2.

Similar to $p = 1\%$ results, it is possible to view that the estimation of the HTC have a detachment from the real values especially on the initial timesteps, what is attenuated at highest timesteps. As in linear case (session 6.2.1), even though there was a greater spread of the σ_ρ using greater noise levels, it's possible see that the standard deviation converges to $\sigma_\rho \cong 0.135$. This observation, added to the good filtering and estimated results, clearly shows that the MFS-PF approach provides stable numerical solutions to the inverse Robin problems with radiation boundary.

The computational cost for 400 particles were on average 3357 seconds, indicating that the time to propagate each particle through MFS to the problem was inferior than 0.84 seconds, representing an increase of 195% in comparison of linear case in session 6.2.1.

7 GENERAL CONCLUSIONS AND FUTURE WORKS

In this present work an investigation about the parabolic MFS to linear and nonlinear boundary conditions was made. A sequential MFS was developed and shown good performance in the linear cases, with and higher RMSE and computational cost in nonlinear cases.

A combined MFS-PF was implemented. This approach has produced accurate and stable results in the estimation of time-dependent HTCs. When radiation is present, the computational cost increases due to the nonlinearity in the corresponding boundary condition. The influence of the number of particles, as well as of the measurement noise have been analyzed. As expect, as the noise decreases or as the number of particles increases, the results improve, with narrow credible intervals. Also, as the number of particles increases, the results become more concentrated around the true value of the HTC.

Non-standard measurements were used the estimation procedures, and presented good results in comparation to the standard measurements. This remark is interesting principally for problems that uses Cauchy data to estimate state and parameters, since many times the obtainment of Cauchy data is impracticable.

In the cases where previous results were disponible, the MFS-PF has yielded comparable results in terms of accuracy, stability, and width of the credibility intervals, with additional improved features such as being less time consuming and preserving the physical non-negativity of HTC.

All in all, this is an initial study. The SIR is a well-known tool for state-estimation problems, but the MFS for parabolic problems lacks of studies to make it more predictable in relation to the source points placement and the number of collocation points.

As suggestion, future works can extend this approach to non-homogenous parabolic problems using RBFs or the DRM to deal with the particular solution, and extend this method for highest dimensions, as in three-dimensional spatial domain $T(x, y, z, t)$.

Other suggestion is applying the sequential MFS-PF into real problems. As this work uses dimensionless diffusivity, therefore all problems were developed in dimensionless way, the diffusivity influence in the approach was not investigated.

8 REFERENCES

[1] T. T. M. Onyango, D. B. Ingham, D. Lesnic and M. Slodicka, "Determination of a time-dependent heat transfer coefficient from non-standard boundary measurements," *Mathematics and Computers in Simulation,* pp. 1577-1584, 2009.

[2] M. Slodicka, D. Lesnic and T. T. M. Onyango, "Determination of a time-dependent heat transfer coefficient in a nonlinear inverse heat conduction problem," *Inverse Problems in Science and Engineering,* vol. 18, no. 1, pp. 65-81, 2010.

[3] P. L. Masson, T. Loulou and E. Artioukhine, "Estimation of a 2D convection heat transfer coefficient during a test: Comparision between two methods and experimental validation," *Inverse Problems in Science and Engineering,* no. 17, pp. 594-617, 2004.

[4] M. F. Valle, M. J. Colaço and F. S. Netto, "Estimation of the heat transfer coefficient by means of the method of fundamental solutions," *Inverse Problems in Science and Engineering,* vol. 16, no. 6, pp. 777-795, 2008.

[5] A. Mocerino, M. J. Colaço, F. Bozzolini and S. Ranieri, "Filtered reciprocity functional approach to estimate internal heat transfer coefficients in 2D cylindrical domains using infrared rhermography," *International Journal of Heat and Mass,* pp. 1181-1195, 2018.

[6] F. C. Hamilton, M. J. Colaço, R. N. Carvalho and A. J. K. Leiroz, "Heat trasfer coefficient estimation of an internal combustion engine using particle filters," *Inverse Problems in Science and Engineering,* vol. 3, no. 22, 2013.

[7] B. Jin and Y. Zheng, "Boundary knot method for some inverse problems associated with the Helmholtz equation," *International Journal for Numerical Methods in Engineering,* no. 62, pp. 1636-1651, 2005.

[8] K. Parand and J. A. Rad, "Kansa method for the solution of a parabolic equation with an unknown spacewise-dependent coefficient subject to an extra measurement," *Computer Physics Communications,* pp. 582-595, 2013.

[9] Y. C. Hon and W. Chen, "Boundary knot method fo 2D and 3D Helmholtz and convection-diffusion problems under complicated geometry," *International Journal for Numerical Methods in Engineering,* pp. 1931-1948, 2003.

[10] A. Doucet, S. Godsill and C. Andrieu, "On sequential Monte Carlo Sampling methods for Bayesian filtering," *Statistics and Computing,* no. 10, pp. 197-208, 2000.

[11] R. Kalman, "A new approach to linear filtering and prediction problems," *ASME Journal of Basic Engineering,* no. 82, pp. 35-45, 1960.

[12] J. Kaipio and E. Somersalo, Statistical and Computational Inverse Problems, Berlin: Springer, 2004.

[13] S. M. Arulampalam, N. Gordon and T. Clapp, "A tutorial on particle filters for online non-linear/non-Gaussian Bayesian tracking," *IEEE Transactions on Signal Processing,* no. 50, pp. 174-188, 2001.

[14] J. Kaipio, S. Duncan, A. Seppanen, E. Somersalo and A. Voutilainen, Handbook of Process Imaging for Automatic Control, Boca Raton, Florida: CRC Press, 2005.

[15] C. Andrieu, A. Doucet, S. Sumeetpal and V. Tadic, "Particle methods for charge detection," in *Proceedings of IEEE*, 2004.

[16] J. M. Hammersley and D. C. Hanscomb, Monte Carlo Methods, New York: Chapman, 1964.

[17] N. Gordon, D. Salmond and A. F. M. Smith, "Novel approach to nonlinear and non-Gaussian Bayesian state estimation," *Instituition of Electrical Engineers,* no. 140, pp. 107-113, 1993.

[18] H. R. B. Orlande, G. S. Dulikravich and M. J. Colaço, "Application of Bayesian filters to heat conduction problems," *EngOpt 2008 - International Conference on Engineering Optimization,* 2008.

[19] T. Abdelhamid, A. H. Elsheikh, A. Elazab, S. W. Sharshir, E. S. Selima and D. Jiang, "Simultaneous reconstruction of the time-dependent Robin coefficient and heat flux in

heat conduction problems," *Inverse Problems in Science and Engineering,* pp. 1231-1248, 2017.

[20] V. D. Kupradze and M. A. Aleksidze, "The method of functional equations for the approximate solution of certain boundary value problems," *USSR Computational Mathematics and Mathematical Physics,* vol. 4, no. 4, p. 82–126, 1964.

[21] R. Mathon and R. L. Johnson, "The approximate solution of elliptic boundary-value problems by fundamental solutions," *SIAM,* vol. 14, no. 4, p. 638–650, 1977.

[22] A. Bogomolny, "Fundamental solutions method for elliptic boundary value problems," *Journal of Numerical Analysis,* vol. 22, no. 4, pp. 644-669, 1985.

[23] C. J. S. Alves and C. S. Chen, "A new method of fundamental solutions applied to," *Advances in Computational Mathematics,* vol. 23, no. 1-2, pp. 125-142, 2005.

[24] C. J. S. Alves and A. L. Silvestre, "On the application of the method of fundamental solutions to nonlinear partial differential equations," *Engineering Analysis with Boundary Elements*, no. 92, pp. 267-274, 2018.

[25] D. L. Young, C. L. Chiu , C. M. Fan, C. C. Tsai and Y. C. Lin, "Method of fundamental solutions for multidimensional Stokes equations by the dual-potential formulation," *European Journal of Mechanics - B/Fluids,* pp. 877-893, 2006.

[26] P. W. Patridge, C. A. Brebbia and L. C. Wrobel, "The Dual Reciprocity Boundary Element Method," in *Computational Mechanics Publications*, Southampton, 1992.

[27] M. A. Golberg and C. S. Chen, "The method of fundamental solutions for potential, Helmholtz and diffusion problems," in *Boundary Integral Methods: Numerical and Mathematical Aspects*, 1999, pp. 105-176.

[28] S. S. Valtchev and N. C. Roberty, "A time-marching MFS scheme for heat conduction problems," *Engineering Analysis with Boundary Elements*, pp. 480-493, 2008.

[29] D. L. Young, M. H. Gu and C. M. Fan, "The time-marching method of fundamental solutions for wave equations," *Egineering Analysis with Boundary Elements,* pp. 1411-1425, 2009.

[30] C. Y. Lin, M. H. Gu and D. L. Young, "The time-marching method of fundamental solutions for multi-dimensional telegraph equations," *Computers, Materials & Continua,* vol. 18, no. 1, pp. 43-68, 2010.

[31] D. L. Young, C. C. Tsai, K. Murugesan, C. M. Fan and C. W. Chen, "Time-dependent fundamental solutions for homogeneous diffusion problems," *Engineering Analysis with Boundary Elements*, pp. 1463-1473, 2004.

[32] S. Chantasiriwan, "Methods of fundamental solutions for time dependent heat conduction problems," *International Journal for Numerical Methods in Engineering,* vol. 1, no. 66, pp. 147-165, 2006.

[33] B. T. Johansson and D. Lesnic, "A method of fundamental solutions for transient heat conduction," *Engineering Analysis with Boundary Elements,* no. 9, pp. 697-703, 2008.

[34] B. T. Johansson and D. Lesnic, "A method of fundamental solutions for transient heat conduction in layered materials," *Engineering Analysis with Boundary Elements,* no. 33, pp. 1362-1367, 2009.

[35] J. A. Kolodziej and M. Mierzwiczak, "Transient heat conduction by different versions of theMethod of Fundamental Solutions – a comparison study," *Computer Assisted Mechanics and Engineering Sciences,* no. 17, pp. 75-88, 2010.

[36] B. T. Johansson, D. Lesnic and T. H. Reeve, "A method of fundamental solutions for two-dimensional heat conduction," *International Journal of Computer Mathematics,* vol. 8, no. 88, p. 1697–1713, 2011.

[37] B. T. Johansson, D. Lesnic and T. Reeves, "A method of fundamental solutions for the radially symmetric inverse heat conduction problems," *International Communications in Heat and Mass Transfer,* no. 39, pp. 887-895, 2012.

[38] P. A. Ramachandran, "Method of fundamental solutions: singular value decomposition analysis," *Communications in Numerical Methods in Engineering,* vol. 18, no. 11, pp. 789-801, 2002.

[39] J. K. Grabski, "On the sources placement in the method of fundamental solutions for time-dependent heat conduction problems," *Computers & Mathematics with Applications,* 2019.

[40] C. E. P. Kopperschmidt, B. H. M. Margotto, W. B. Silva and J. C. S. Dutra, "Source points placement in the method of fundamental solutions for parabolic problems," *Anais do XXII Encontro Nacional de Modelagem Computacional e o X Encontro de Ciência e Tecnologia de Materiais,* pp. 2073-2082, 2019.

[41] N. S. Mera, "The method of fundamental solutions for the backward heat conduction problem," *Inverse Problems in Science and Engineering,* pp. 65-78, 2005.

[42] T. H. Reeve, The method of fundamental solutions for some direct and inverse problems, Birmingham: Thesis. School of Mathematics, Engineering and Physical Sciences, University of Birmingham, 2013.

[43] P. C. Hansen, "Analysis of discrete ill-posed problems by means of L-curve," *SIAM,* pp. 561-580, 1992.

[44] L. Yan, F. Yang and C. Fu, "Bayesian inference approach to identify a Robin coefficient in on-dimensional parabolic problems," *Journal of Computational and Applied Mathematics,* no. 231, pp. 840-850, 2009.

[45] A. Doucet, N. Freitas and N. Gordon, Sequential Monte Carlo Methods in Practice, Berlin: Springer, 2001.

[46] F. Campillo and V. Rossi, "Convolution particle filter for parameter estimation in general state-space models," *IEEE Transactions on Aerospace and Electronic Systems,* no. 55, pp. 1063-1072, 2009.

[47] P. Mayback, Stochastic models, estimation and control, New York: Academic Press, 1979.

[48] J. Liu and M. West, "Combined parameter and state estimation in simulation-based filtering.," in *Sequential Monte Carlo Methods in Practice. Statistics for Engineering and Information Science,* Springer, 2001, pp. 197-223.

[49] M. P. Rios and H. F. Lopes, "The extended Liu and West Filter: parameter learning in Markov switching stochastic volatily models," in *State-Space Models*, Springer, 2013, pp. 23-62.

[50] W. B. Silva, M. C. Rochoux, H. R. B. Orlande, M. J. Colaço, O. Fudym, M. El-Hafi, B. Cuenot and S. Ricci, "Application of particle filters to regional-scale wildfire spread," *High Temperatures High Pressures,* no. 43, pp. 425-440, 2014.

[51] L. S. F. Salardani, L. P. Albuquerque, J. M. J. Costa, W. B. Silva and J. C. S. Dutra, "Particle filter-based monitoring scheme for simulated bio-ethylene production process," *Inverse Problems in Science and Engineering,* no. 27, pp. 648-668, 2018.

[52] B. Ristic, S. Arulampalam and N. Gordon, Beyond the Kalman Filter, Boston: Artech House, 2004.

[53] A. Kong, J. S. Liu and W. H. Wong, "Sequential imputations and Bayesian missing data problems," *Journal of the American Statistical Association,* vol. 89, no. 425, pp. 278-288, 1994.

[54] A. C. S. R. Dias, W. B. da Silva and J. C. S. Dutra, "Propylene polymerization reactor control and estimation using a particle filter and neural network," *Macromolecular Reaction Engineering,* vol. 11, pp. 1-20, 2017.

[55] F. Yang, L. Yan and T. Wei, "The identification of a Robin coefficient by a conjugate gradient method," *International Journal of Numerical Methods in Engineering,* vol. 78, no. 7, pp. 800-816.

[56] R. Marques, W. B. Silva, R. Hoffmann, J. S. Dutra and F. Coral, "Sequential state inference," *Computational and Applied Mathematics,* no. 37, pp. 220-236, 2017.